Photocatalytic Chlorine Production from Iron Chlorides in Atmospheric Aerosols: Strategies for Quantifying Methane and Tropospheric Ozone Control

Maarten van Herpen[1], Luisa Pennacchio[2], Chloe Brashear [3], Marie K. Mikkelsen [2], Alfonzo Saiz-Lopez [4], Thomas Röckmann[3], Matthew S. Johnson[2]

[1]Acacia Impact Innovation BV, Acacialaan 9, 5384 BB, Heesch, The Netherlands.
[2]Department of Chemistry, University of Copenhagen, Universitetsparken 5, DK-2100 Copenhagen, Denmark.
[3]Institute for Marine and Atmospheric Research Utrecht, Utrecht University, 3508 TA Utrecht, The Netherlands.
[4]Department of Atmospheric Chemistry and Climate, Institute of Physical Chemistry Blas Cabrera, CSIC, Madrid 28006, Spain.

Key Points:

- Using iron-salt aerosols to generate chlorine may cut methane, but field studies are needed to characterize safety and efficiency.
- Indicators for Cl^0 production in ship or iron plumes include photoactive iron, CO:ethane ratio, Cl_2, $ClNO_3$, $ClNO_2$, HOCl and ClO.
- This study enables field studies of the viability of iron-salt aerosols as a methane removal technology and the Cl production efficiency.

Corresponding author: Matthew S. Johnson, msj@chem.ku.dk

Abstract

It was recently discovered that chlorine is produced photocatalytically from mineral dust-sea spray aerosols, impacting methane and tropospheric ozone, and an evaluation was made of the climate and environmental impact of a chlorine-based intervention to draw down methane. The generation of chlorine by the iron chlorides $Fe(III)Cl_n^{(3-n)}$ will also occur due to iron present in shipping plumes. To study efficiency and environmental implications, there is a need for additional information about the behavior of the process under a range of atmospheric conditions. Here we use box modeling to evaluate whether it is possible to experimentally observe this mechanism in a ship's plume, or in a plume of pure iron dust, emitted for example from a tower. Detection limits for Cl, Cl_2, HOCl, ClO, $ClNO_3$, $ClNO_2$, CO, C_2H_6, $\delta^{13}C(CO)$ and CH_2O are determined based on values from the literature. We find that the most promising and low-cost experimental indicators of Cl^0 production are the concentration of photoactive iron and the CO:ethane ratio, and Cl_2 is a useful indicator if cost is not a limitation. For ships with high NO_x emissions, $ClNO_2$ and $ClNO_3$ could also potentially be used, and for towers emitting Fe without NO_x the concentration of HOCl and ClO could be used. $\delta^{13}C(CO)$ is a very direct method to detect methane removal, but only gives a clear signal for high iron emissions.

Plain Language Summary

Researchers have discussed a potential solution to tackle rising atmospheric methane levels, a major contributor to global warming. Iron-salt aerosols, produced naturally in the atmosphere today from mineral dust and sea spray, could potentially be used as a cost-effective intervention to remove methane. However, there are significant questions about the safety, efficacy and appropriate conditions for any such approach.Our study evaluates methods of characterising the impact of such an intervention by evaluating chlorine production in various atmospheric conditions, specifically in ship plumes or when emitted from towers.

We assess methods that could be used in field studies, including measuring photoactive iron concentration, the CO:ethane ratio, and advanced species detection methods. Field studies are crucial to determine the viability of iron-salt aerosols in combating global warming, balancing potential benefits with safety considerations. This research provides a vital step towards understanding and implementing innovative solutions to mitigate climate change.

1 Introduction

Methane is a potent greenhouse gas, currently responsible for more than 1/3 of global warming since pre-industrial times (IPCC, 2021), and it is atmospheric burden continues to increase with a new record set in 2022 (Lan et al., 2024). The pathways assessed by the IPCC that stay below 1.5 °C of global warming by 2050 require substantial reductions of methane emissions (IPCC, 2021; Rogelj & Lamboll, 2024). The main way to achieve this is to reduce methane emissions from especially agriculture, fossil fuels and waste. According to Höglund-Isaksson et al. (2020), the maximum potential for reduction in emissions is limited to 30-45 % by 2030 and 50 % by 2050. This leaves a large amount of methane that cannot be mitigated unless new currently unknown mitigation technologies are discovered, or if a technology is developed to remove methane from the atmosphere, similar to carbon dioxide removal technologies.

While the Global Methane Pledge signed by many countries may contribute to reducing emissions (European Commission, 2023 November 2021, Brussels), it is not sufficient to prevent 1.5 °C of global warming by 2050 (Rogelj & Lamboll, 2024). In addition, due to global temperature rise the biological emissions of methane are increasing substantially (Kleinen et al., 2021; Nisbet et al., 2023), which can not be addressed through

anthropogenic methane emission reductions. According to recent work, atmospheric methane removal has the potential to reduce global average temperature by 0.4-1 °C (Smith & Mathison, 2024; Abernethy et al., 2021; Staniaszek et al., 2021), helping to avoid substantial levels of additional warming by mid-century (Smith & Mathison, 2024), and may reduce climate risks (Abernethy & Jackson, 2024).

To achieve these benefits, thousands of megatons of atmospheric methane removal will be required urgently (Smith & Mathison, 2024). Such scale and time to scale can likely only be achieved through open-system approaches (Abernethy & Jackson, 2024; Pennacchio, Mikkelsen, et al., 2024), such as atmospheric oxidation enhancement by lofting Iron Salt Aerosols (ISA) (Oeste et al., 2017; Meyer-Oeste, 2014; Ming et al., 2021)) into the atmosphere to catalytically generate chlorine radicals that oxidize methane. However, because such open-systems are tougher to verify and have higher risks of unintended consequences, quantification and observations to verify any hypothetical future methane removal is important to enable governance approaches.

Research into Iron Salt Aerosols (ISA) (Oeste et al., 2017; Meyer-Oeste, 2014; Ming et al., 2021) is still in an early phase, with only few demonstrations in the laboratory (Wittmer, Bleicher, & Zetzsch, 2015; Wittmer, Bleicher, Ofner, & Zetzsch, 2015; Wittmer & Zetzsch, 2017; Mikkelsen et al., 2024). There are significant questions regarding the safety, efficacy and appropriate conditions for any such approach (Gorham et al., 2024). According to global modeling, low-intensity chlorine emissions by ISA can under certain conditions cause methane to increase due to destruction of ozone that leads to decreased OH (van Herpen et al., 2023; Li et al., 2023; Meidan et al., 2024; Pennacchio, van Herpen, et al., 2024). Other potential adverse impacts that need to be studied are iron aerosols causing warming by absorbing radiation (Meidan et al., 2024) and stratospheric ozone destruction (Li et al., 2023) However, recently iron salt aerosols have been reported in Sahara dust mixed with sea spray (van Herpen et al., 2023), creating opportunities for studying some of these questions.

The main source of anthropogenic iron in the atmosphere is shipping, due to metal impurities found in fuel (Agrawal et al., 2008), estimated at below 2 Gg Fe/yr (Ito, 2013). It is hypothesized that these anthropogenic emissions of soluble iron will mix with sea-salt aerosols over the ocean, creating iron-salt aerosols that would produce chlorine, removing methane from the atmosphere (Oeste et al., 2017; Ming et al., 2021). Emissions from shipping change depending on maritime policy (Čampara et al., 2018) and the choice and composition of fuel. Therefore, more research must be conducted regarding the formation of ISA in shipping plumes. A switch to novel shipping fuels such as methanol or ammonia (Tomos et al., 2024) (which don't contain iron) could reduce iron emissions leading to lower chlorine production, but there is also a potential for increasing methane removal by enhancing iron emissions by ships.

There is an increasing interest in conducting a field study into Cl production from iron emissions. Proposed dispersion methods include the addition of $FeCl_3$ into the hot exhaust of ships (leveraging the buoyancy to lift up the particles), or releasing the $FeCl_3$ from uplift towers (Oeste et al., 2017). Sturtz et al. (2022) employed a modeling approach for the potential environmental impacts associated with a hypothetical small-scale field test consisting of seeding cargo-ship exhaust plumes with iron salt aerosols. No significant impacts were identified in this assessment, but the authors did not assess whether the amount of iron released would lead to a detectable amount of chlorine production.

One category of ship plume field studies uses instruments at a fixed location near busy shipping channels, using the automatic identification system (AIS) to identify ships and measure the plume emissions as they pass the instrument (Ault et al., 2010; Kivekäs et al., 2014; Ausmeel et al., 2020). Another type of study creates a concentration map by taking several measurements inside a plume (G. Chen et al., 2005). The advantage of in-plume measurement is that accurate information is acquired about in situ chem-

istry, free of surface interference, while measurements from a fixed location are easier to implement. For in-plume measurements, a research aircraft (Andrés Hernández et al., 2022; G. Chen et al., 2005) or drone (Zhou et al., 2023) can fly through the ship plume while taking measurements using a variety of instruments on board. Another way to create a concentration map of a ship plume is using Multi-Axis Differential Optical Absorption Spectroscopy (MAX-DOAS) to scan the ship plume (Cheng et al., 2019).

In this study, we combine a time-dependent photochemical box model with plume dispersion to evaluate whether it is possible to experimentally observe chlorine production from iron-salt aerosols in a ship plume. We perform the same evaluation for a plume of iron salt aerosols from a source that does not emit NO_x.

2 Method

2.1 Box model

We employed a similar approach as used by Song et al. (2003), who studied NO_x/HO_x chemistry within a ship plume by combining a plume dispersion algorithm with a time-dependent photochemical box model. The box model is initialized using background marine conditions, after which we allow it to run for 16 days to reach quasi-steady state conditions for the time varying species. Subsequently, we add a pulse of NO, CO, ethane and ISA particles on day 17 (representing emissions from the ship), which then disperse into the background.The timing of the pulse of ship emissions in our model is done at sun-rise. We selected this time to ensure that sunlight is available for a long as possible during the day, allowing Cl_2 to still be produced far away from the ship. At the same time this will lead to a low-estimate for Cl_2 production close to the ship, which would be higher for a mid-day emission.

The ISA particles generate Cl_2 with the same efficiency as was found for mineral dust by van Herpen et al. (2023), producing 11 photochemistry cycles per hour (5.5 Cl_2 per hour) at maximum sunlight, which is on the low end of the efficiency measured in smog chamber studies by Wittmer and Zetzsch (2017) of 6 to 78 per hour. For example, a photo-active iron concentration of 10 ng/m^3 corresponds to 1.8×10^{-13} mol Fe/cm^3, which is multiplied by 5.5 Cl_2 per hour per Fe atom, resulting in 9.9×10^{-13} mol Cl_2/hour/cm^3 $= 1.7 \times 10^8$ molecules Cl_2/cm^3/s. We multiply this maximum value with a diurnal profile (a number between 0 and 1).

A full overview of reactions in our photochemistry box model, which is built in the compiler program Kintecus (Ianni, 2017), can be found in the Appendix. The model contains all the reactions that Song et al. (2003) identified as the most important for boundary layer ship plume chemistry. This includes all the inorganic reactions of the atmosphere and the full oxidation mechanism of CH_4 and dimethyl sulfide (DMS), as obtained from the Master Chemical Mechanism, MCM v3.3.1 (*Master Chemical Mechanism, MCM v3.2*, 2023). The model does not include non-methane VOC chemistry, but we included the basic reactions for ethane with OH and Cl to be able to track the CO:ethane ratio in the ship plume. In addition, the model contains the ClO_x reactions and key deposition rates, including the uptake and hydrolysis of $ClONO_2$ (yielding HNO_3 and HOCl), and the reactive uptake of HOCl (yielding Cl_2). Bromine and iodine chemistry is not included in the main model runs, because it was found to have low impact on the ship plume chemistry relevant for our conclusions. A sensitivity analysis was done using bromine and iodine chemistry based on (Saiz-Lopez et al., 2006; Hossaini et al., 2016; Saiz-Lopez et al., 2014). We use the same photochemistry box model in Pennacchio, van Herpen, et al. (2024), where further details on bromine chemistry impact, including a comparison with the Community Earth System Model (Meidan et al., 2024) be found.

Plume dispersion in our model was done using the method described by Song et al. (2003), in which the concentration change for a species due to dilution is calculated

using:

$$C_{i,t+1} = D_t C_{i,t} + (1 - D_t) C_{i,b} \quad (1)$$

in which D_t is the calculated dilution factor representing a rate of dispersion per time step at time t after emission, which we calculated based on pre-defined scenarios with known plume dispersion either from modeling or from measurements. $C_{i,b}$ is the background concentration of species i, for which we used the quasi-steady state concentration during the last 24 hours of the stabilization time. $C_{i,t}$ is the concentration of species i at time t (in s). To assess if it is possible to detect Cl_2 production from iron-salt aerosols in an emission plume, we used our box model to estimate the concentration of Cl_2, ClO, HOCl, $ClNO_3$, $ClNO_2$, CH_2O, CO isotope changes and CO:ethane ratio changes along the centerline of the ship's plume. The relative wind speed (see table 2 in section 2.2) is used to convert the time after emission into distance.

To simplify the analysis, we assume that the iron is added post-combustion into the ship plume exhaust stream as $FeCl_3$, which implies that 100% of the iron is photoactive, and can produce Cl immediately after emission. Ship iron emissions resulting from iron in the fuel have an uncertain photoactive fraction (Meidan et al., 2024) and may require atmospheric processing before becoming photoactive, and this is excluded in our model.

We used a NO emission of 20 g/kg fuel(G. Chen et al., 2005), a relatively high CO emission of 12 g/kg fuel(Winnes & Fridell, 2009) (to simulate a worst case interference from the ships CO emissions), and a CO:ethane ratio in the emission of 200 (Read et al., 2009). The background CO level was set to 90 ppb, with a CO:ethane ratio of 50 (Read et al., 2009). To calculate $\delta^{13}C(CO)$, we assumed a background value of -30 ‰ , a value emitted by the ship of -25 ‰ (Bergamaschi et al., 2000), and a value for CO produced from Cl oxidation of methane of -110 ‰ (Röckmann et al., 2024).

2.2 Scenarios

Our scenarios combine a dispersion scenario (expressed with capital letters A-H) with an iron emission scenario (expressed with lower case letters a-c).

Our lowest iron emission scenario "a" (see Table 1) adds 0.021 g iron per second to the exhaust, which is similar to a ship burning 3.75 ton/hour of fuel with a typical 20 ppm Fe content. Since 300 ppm ferrocene is the highest fuel concentration that still improves engine emission conditions ("Improving performance and emissions characteristics of compression ignition engine: Effect of ferrocene nanoparticles to diesel-biodiesel blend", 2020), we increase iron emissions by 10× in scenario "b" without changing any of the other emissions. Our highest Fe emission scenario "c" increases iron emissions again by 10×, and is therefore higher than what could be expected from ship combustion Fe emissions. However, note that in our model $FeCl_3$ is added to the ship plume exhaust, and we do not account for iron-oxide emitted by the ship itself, assuming only a low fraction is photo-active. Thus, while we based the iron emission scenarios on typical combustion emissions, in our model the iron is emitted as 100% photoactive $FeCl_3$ that is emitted into the exhaust stream, with the emission expressed as the amount of elemental iron within the emitted $FeCl_3$.

Table 1. Iron-salt aerosol emission scenarios

Scenario label	Fe emission/(g/s)
0	0
a	0.021
b	0.21
c	2.1

We explored the feasibility of a field study using several dispersion scenarios ranging from A to H (see Table 2.2), and we include different meterological stability classses (Hanna et al., 1981). Dispersion in scenario A and D is based on Song et al. (2003) and G. Chen et al. (2005), respectively, while in scenarios B, C, F and G the dispersion of the ship plumes were calculated using the HYSPLIT atmospheric transport and dispersion model through the NOAA READY tool (Rolph et al., 2017) . Because this tool only calculates dispersion up to 50 km, we assumed that the plume expansion continues at the same rate beyond this distance.

Scenario A is used to compare our model output with model results in Song et al. (2003), from which we used scenario IIb. This scenario uses a mixing height of 700 m relative wind speed of 5 m/s, meterological stability class E (slightly stable), and NO_x emission of 10 g/s, with a background NO_x concentration of 7 ppt, and O_3 of 18.5 ppb. This stability class will result in the slowest plume dispersion of all our scenarios. We derived the plume dispersion rates from Song et al. (2003), using their reported nighttime NO_x concentration and instant NO_x lifetime curves.

Scenario B is a general low relative wind-speed scenario of 2.6 m/s and a meteorological stability class C (slightly unstable).

Scenario C is the hypothetical field study near the island Bonaire that was assessed by Sturtz et al. (2022). We used the deposition rates that Sturtz calculated for Fe and HCl emissions to calculate the plume dilution factor, and compared the result with the output of NOAA READY for 8 m/s and stability class D (Neutral). The dilution factor was in agreement between these two methods, but because NOAA READY provides output beyond 6 km, we used NOAA READY as input for our box model.

Scenario D uses measurement data by G. Chen et al. (2005), in which a ship plume was sampled using an aircraft, with wind speed of 10 m/s. We will assess whether this field study could have detected Cl_2 production from ISA in the ship's plume. Because the observational data by G. Chen et al. (2005) is only available starting at 40 minutes after emission, we used a NOAA READY model for the first 40 minutes.

Scenarios E, F, G and H model iron emissions from a point source of iron dust, without the pollution emissions associated with ship emissions. This scenario represents a field study using emissions of mineral dust, iron-oxide dust, or $FeCl_3$, and we will sometimes refer to this as tower emissions instead of ship emissions. Scenarios E, F, G and H were performed using the dilution factors from scenarios A, B, C and D, respectively. In these scenarios there is no pulse of NO_x, CO or ethane released, since the dust is not emitted through fuel burning.

Background conditions are assumed to be similar for all scenarios (remote marine boundary layer).

Table 2. Overview of the 8 different plume scenarios (Sce.) that represent ship plume and tower emission scenarios. With the relative wind speed in m/s, Stability Class (STB Class)(Hanna et al., 1981), Mixing Height (MH) in m, the source of NO_x in g/s [a], the background of NO_x in ppt (Bkgd NO_x) and the background of O_3 in ppb (Bkgd O_3).

Sce.	Wind /(m/s)	STB Class	MH /m	NO_x emission /(g/s)	Bkgd NO_x /ppt	Bkgd O_3 /ppb	References
A	5	E	700	10	7	19	Song et al. (2003)
B	2.6	C	681	21	53	14	-
C	8	D	400	21	53	14	Sturtz et al. (2022)
D	10	D	300	21	53	14	G. Chen et al. (2005)
E	5	E	700	0	53	14	-
F	2.6	C	681	0	53	14	-
G	8	D	400	0	53	14	-
H	10	D	300	0	53	14	-

[a] Using NO emission of 20 g/kg fuel, and CO emission of 12 g/kg fuel means that CO emissions in our model are 60% of NO emissions

2.3 Detection limits of investigated species

2.3.1 Photoactive iron

Several methods are available to measure iron in aerosols. Iron-salt aerosols can be detected as photo-active iron in aerosol samples that can be collected by drawing air through a filter inside a ship's plume. The concentration of photoactive iron can be detected as a photo-reducible fraction of soluble iron (Y. Chen & Siefert, 2003; X. Zhu et al., 1993; X. R. Zhu et al., 1997). This is done by determining the concentration of Fe(II) before and after the reducible fraction of Fe(III) is reduced to Fe(II). Fe(II) can be measured colorimetrically by complexation with ferrozine (Viollier et al., 2000).

The reduction of Fe(III) to Fe(II) is performed by either using hydroxylamine hydrochloride reduction, or by exposing the sample to direct sunlight to photo-reduce the Fe(III) (Y. Chen & Siefert, 2003). Examples of the detection of photo-active iron in the atmosphere are the measurement of the diel cycle of Fe(II) at Barbados by X. R. Zhu et al. (1997) and the detection of photo-active iron in ship-based studies across the North Atlantic (Y. Chen & Siefert, 2003). The detection limit for photoactive iron in these studies was in the order of 1 ng/m^3.

2.3.2 Cl detection with radical clock method

The so-called radical clock approach can be used to quantify the role of chlorine chemistry inside and outside a plume (Baker et al., 2011, 2016). Chlorine atoms react with certain hydrocarbons more quickly than others, and this pattern is different from how hydroxyl radicals, the main atmospheric oxidant, react. The quantification can be realized by collecting air samples for analysis by gas chromatography. Examples of this methodology include observations of chlorine chemistry in a volcanic plume (Baker et al., 2011) and in the pollution outflow of Asian cities (Baker et al., 2016), based on which we estimate a detection limit of on average 1×10^4 Cl cm^{-3} over 24 hours exposure time, or 1×10^5 Cl cm^{-3} for 2.4 hours of exposure.

2.3.3 Cl_2 and HOCl

Lawler et al. (2011) detected HOCl and Cl_2 in atmospheric air at Cape Verde using chemical ionization tandem mass spectrometry (CIMS-MS) via the formation of a Br^- adduct. The instrument detection limits were approximately 30 ppt HOCl and 1 ppt Cl_2 for the first three days of the study, and 5 ppt HOCl and 2 ppt Cl_2 during the last four days. Chemical ionization mass spectrometers have been carried on board research aircraft (Yuan et al., 2016; Le Breton et al., 2012), including an aircraft CIMS study of ship plumes (G. Chen et al., 2005), but no CIMS measurements of in-plume halogen chemistry have been performed to date.

2.3.4 ClO

ClO can be detected with long-path DOAS (Stutz et al., 2002) which has the advantage that it generates a real-time signal, and can scan different parts of a plume. To detect ClO with LP-DOAS, the concentration should be above 1 ppt and preferably above 5 ppt (Stutz et al., 2002). Alternatively, ClO can also be measured with CIMS, with a similar detection limit (Custard et al., 2016) (2.6 ppt for 2.8 s integration time). We will use 5 ppt in our analysis.

2.3.5 $ClNO_3$

$ClNO_3$ can be detected in the atmosphere with a detection limit of less than 3 ppt using CIMS on board of aircraft (Marcy et al., 2005). $ClNO_3$ can also be detected using mid-infrared spectrometry for studies of stratospheric $ClNO_3$ via absorptions in the wavelength range of 5.7 μm to 12.8 μm (at 779, 809, 1293 and 1735 cm^{-1}) (von Clarmann & Johansson, 2018).

2.3.6 $ClNO_2$

The detection limit for $ClNO_2$ with CIMS is around 3 ppt for 1 minute integration, and 13 ppt for 1 s (Kercher et al., 2009; Saiz-Lopez & von Glasow, 2012). Based on these numbers we will use a detection limit threshold of 10 ppt, taking into account high time resolution requirements if the CIMS is carried by aircraft into the plume.

2.3.7 CO:ethane ratio

The ratio of CO to ethane is basically equivalent to a radical clock, and could potentially be a very cost effective method using low cost sensors. That is why we model this ratio separately.

The reaction rate coefficients for CO and ethane with OH are approximately the same(Read et al., 2009). In addition, CO and ethane are typically emitted at a fixed ratio by sources(Read et al., 2009). Due to these conditions, the ratio between atmospheric CO and ethane is quite stable if OH is the only relevant sink. However, ethane reacts with Cl whereas CO does not, making the CO-ethane ratio a sensitive metric of Cl radical exposure. The method was used by Read et al. (2009) in Cape Verde, where large seasonal fluctuations in the CO:ethane ratio were measured. These variations could potentially be due to a large seasonal source of Cl, such as the MDSA mechanism reported by van Herpen et al. (2023).

In our simulation, we used a CO:ethane ratio in the ship exhaust of 200 (mole/mole) (Read et al., 2009). The background CO level was set to 90 ppb, with a typical CO:ethane ratio of 50, based on measurements near Cape Verde (Read et al., 2009).

For ethane detection, we use the reported detection limit of 10 ppt for photo-acoustic trace gas detection (van Herpen et al., 2002), while gas chromatography with flame ionization detection has a detection limit of 3 ppt (Read et al., 2009).

2.3.8 $\delta^{13}C(CO)$

The carbon isotopic composition (δ^{13}C) of CO can be used to detect an enhanced Cl radical concentration due to the strong kinetic isotope effect occurring in the reaction of CH_4 + Cl. It has been shown for a range of tropospheric temperatures that Cl reacts about 70 ‰ faster with $^{12}CH_4$, relative to isotopically heavier $^{13}CH_4$(Saueressig et al., 1995). The first stable product of this reaction, CO, shares a carbon with the original methane molecule. Therefore, an isotopic depletion in ambient CO is evident in air masses with enhanced chlorine oxidation of methane. Unlike alternative proxy methods outlined here, δ^{13}C(CO) is directly linked to CH_4 + Cl chemistry.

Measurements of δ^{13}C(CO) reflect even small CO contributions from chlorine oxidation due to the low tropospheric CO background concentration. For example, if only 1 ppb of CO from chlorine oxidation (with $\delta^{13}C_{CO}$ = -110 ‰, Röckmann et al. (2024)) is added to background air (for example CO = 100 ppb and $\delta^{13}C_{CO}$ = -30.0 ‰), an isotopic shift of -0.8 ‰ is detectable:

$$\delta^{13}C_{CO,mix} = \frac{(100 \times -30 + 1 \times -110)}{101} = -30.8‰ \tag{2}$$

$\delta^{13}C_{CO}$ is measured using continuous-flow isotope-ratio mass spectrometry (IRMS) (Pathirana et al., 2015). Analysis requires 100 mL of sample air from a glass flask pressurized to $\sim$ 1.5 bar. Precision of the instrument is monitored by the standard deviation of reference gas sets, which fluctuates between 0.03 – 0.10 ‰ on average. Thus, a change of more than 0.2 ‰ in δ^{13}C(CO) of ambient air is considered statistically significant. The system also accommodates a range of CO mixing ratios by adjusting sample extraction times and/or flow rates.

2.3.9 CH_2O

The extra OH from the NO_x emissions of ships leads to extra CH_4 oxidation within shipping plumes, and this leads to elevated CH_2O concentrations inside the ship plume (Song et al., 2010). In a busy shipping corridor, the increased CH_2O levels from the enhanced methane oxidation can even be observed with satellites from space, such as ESA/ERS-2 GOME (Global Ozone Monitoring Experiment) (Marbach et al., 2009) and TROPOMI (De Smedt et al., 2018). Thus, CH_2O may also be an attractive indicator species for detecting additional methane oxidation by Cl in shipping plumes.

CH_2O can be detected in a ship plume by MAX-DOAS, which can be used to scan through the plume with a detection limit of 50-300 ppt, making it a convenient detection method (Plane & Saiz-Lopez, 2006; Prados-Roman et al., 2020). While MAX-DOAS has been demonstrated in ship plumes ((Cheng et al., 2019)), the high aerosol levels in ship plumes will adversely affect the detection limit. Therefore the detection limit should be expected to be worse close to the ship, when aerosol levels are still high. Alternatively, CH_2O detectors could be used at a fixed location, with a detection of about 100 ppt(Wu et al., 2023). We will use 100 ppt in our analysis.

3 Results

Table 3. Different stages of ship plume dispersion

Phase 1: O_3 depletion	**Phase 2: O_3 recovery**	**Phase 3: long-term**
Extremely high NO_x.	NO_x reducing due to dispersion.	NO_x slightly elevated after dispersion.
O_3 depleted fully due to $O_3 + NO \rightarrow NO_2 + O_2$.	O_3 recovers above background through NO_2 photolysis.	O_3 increased above background due to extra NO_x.
OH depleted due to depleted O_3.	OH recovers above background along with O_3.	OH increased above background due to extra O_3.
Cl_2 emissions remove NO_x and produce HNO_3, accelerating phase 1.	Cl_2 emissions remove NO_x, accelerating phase 2.	Cl_2 emissions reduce O_3 levels.
Cl_2 emissions increase CH_4 oxidation without further affecting OH/O_3.		Cl_2 emissions reduce OH due to reduced O_3.

Appendix Figure A1 shows that our model output for scenario A agrees with Song et al. (2003), showing the same 3 stages of plume development (see Table 3), early plume with O_3 depletion, mid-range plume with O_3 recovery and rapid OH increase and long-range plume with O_3 production and maximum OH values). The concentrations in our model output show good agreement with Song (Song et al., 2003) for NO_x, O_3, OH, NO_2/NO_x ratio, HNO_3, which gives confidence that our model will be able to predict the species of interest in our study (Cl, Cl_2, ClO, HOCl, $ClNO_3$, $ClNO_2$, HCHO, CO, ethane and $\delta^{13}C(CO)$ in CO). A difference between Song et al. (2003) and our model is that we include ClO_x chemistry which leads to visible differences, especially for NO_3 and N_2O_5. This can be explained by the reaction of $ClO + NO_2 \rightarrow ClNO_3$, where the product photolyses and leads to the formation of NO_3, or hydrolyzes leading to a loss of NO_x (Pennacchio, van Herpen, et al., 2024).

The addition of ISA to the ship plume generates Cl_2 that increases loss of NO_x, which results in increased O_3 and OH levels compared to the scenario without ISA particles. This accelerates the first 2 plume stages of O_3 depletion and recovery, leading to an earlier peak in O_3 and OH. An Fe emission of 0.2 g/s of iron-salt aerosols leads to a peak in [Cl] up to 1×10^6 cm^{-3} in scenario A.

In our scenarios for tower emissions, there is no NO_x emission, due to which these extreme fluctuations in NO_x, O_3 and OH will not occur, making tower scenarios very different from ship scenarios.

Cl atoms are challenging to detect directly, and the next sections discuss indirect methods to detect the Cl chemistry or the presence of ISA in the plume, by measuring other species that are indicative of the Cl chemistry (see Methods).

3.1 Photoactive iron

Throughout this paper, figures will show model output along the center of the plume (also for altitude), as a function of distance from the ship. The time since emission depends on the relative wind speed (for example 5 m/s relative wind speed means that 5000 meters corresponds to 1000 seconds after emission; note that wind speeds vary between scenarios, see Table 2.2).

Figure 1 shows the Fe concentrations in iron-salt aerosols for all plume dispersion scenarios (cf. Table 2.2) in combination with iron emission scenario (a) (our lowest Fe emission scenario). It can be seen that photo-active iron concentrations up to 10 km are a factor of 10 above the detection limit of 1 ng/m^3, and that ship and tower emissions have identical Fe concentrations for the same dispersion profile. Thus, a field study detecting photo-active iron is feasible for all scenarios and should preferably be done within 10 km of the ISA source. If the fraction of photo-active iron in shipping fuel emissions is greater than 10%, it would also be detectable by this method. However,this distance corresponds to a time since emission of 20 - 60 minutes (depending on the relative wind speed), and ISA particles generated via iron emissions by fuel combustion may not yet have appeared within this time. In addition, the disadvantage of photo-active iron measurements is that they do not necessarily prove that the photo-active iron also generates Cl_2. This is only possible with the detection methods presented in the next sections.

It can be seen in Figure 1 that scenarios B and C have similar dispersions as function of distance, but scenario B has lower dispersion with time, which is due to the higher relative wind speed combined with higher stability class for scenario C compared to B. Scenario A leads to the highest Fe concentrations in the dispersed plume (due to relatively low wind speed combined with high stability class), and scenario D will have relatively higher Fe concentrations downwind from the emission source (this scenario is based on observational data and changing conditions led to less dispersion downstream). Scenario D has more fluctuation in the dilution factor, initially following scenario B and C, but then the dilution slows down and it catches up with scenario A. This illustrates the kind of variability that can be expected in the field.

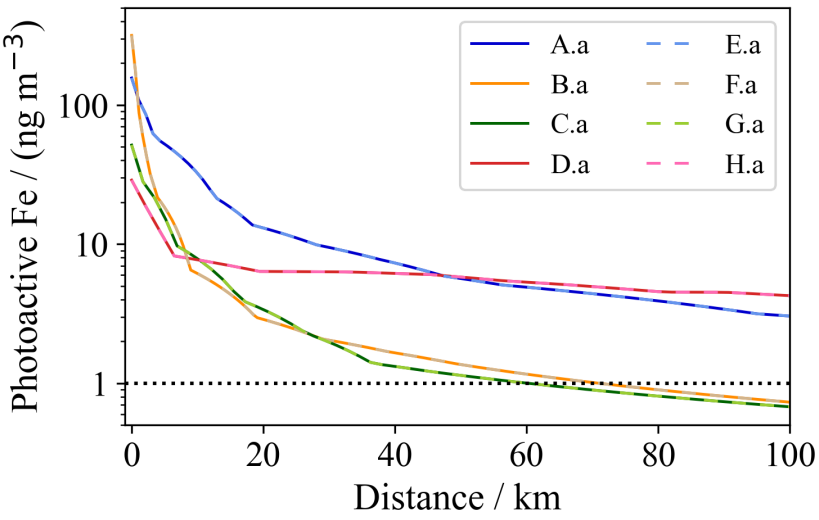

Figure 1. Photoactive iron concentrations for an Fe emission of 0.021 g/s in the various scenarios. Dashed lines are used for scenario E-H to indicate tower emissions and full lines are used for ship emissions. Similar colors are used to indicate the same dispersion scenarios (for example A and E use the same dispersion rate, with A for ship emission and E for tower emission). The detection limit, 1 ng/m^3, is indicated by the dotted black line.

3.2 Cl detection with radical clock method

Our model includes a background HCl concentration of 100 ppt(Wang et al., 2019) that reacts with OH to form Cl, resulting in a background Cl concentration that does not exceed 1×10^3 cm^{-3}, far below the detection limit of $1{\times}10^5$ Cl cm^{-3} for 2.4 hours of exposure. Ship plume NO_x emissions lead to increased OH levels, that result in increased Cl levels up to $6{\times}10^3$ cm^{-3} in scenarios without Fe emission.

Our lowest iron emission rate of 0.02 g/s already leads to Cl concentrations up to $1{\times}10^5$ cm^{-3} (see Figure 2, showing emission scenario a for all dispersion scenarios), with almost identical concentrations for ship and tower emissions with the same dispersion scenario. This increases to 1×10^6 cm^{-3} and 1×10^7 cm^{-3} for 10× and 100× higher iron emissions. Thus, the radical clock method could potentially be used to detect the ISA mechanism in a ship plume with age of 2.4 hour or more.

However, we also note that this method has only been demonstrated for large air masses, while a plume emitted by a ship or tower is a relatively small source. Large amounts of background air will mix into the plume, especially within the first 25 km, greatly diluting the emissions of the ship. This implies that the radical clock method may not work during the initial strong dispersion of the plume, depending on the species that is used for the radical clock. This point is discussed in more detail in the section 3.8. The peak of [Cl] is expected close to the ship (see Figure 2), but beyond 25 km, [Cl] can still be above the detection limit even for the lowest Fe emission scenario of 0.02 g/s.

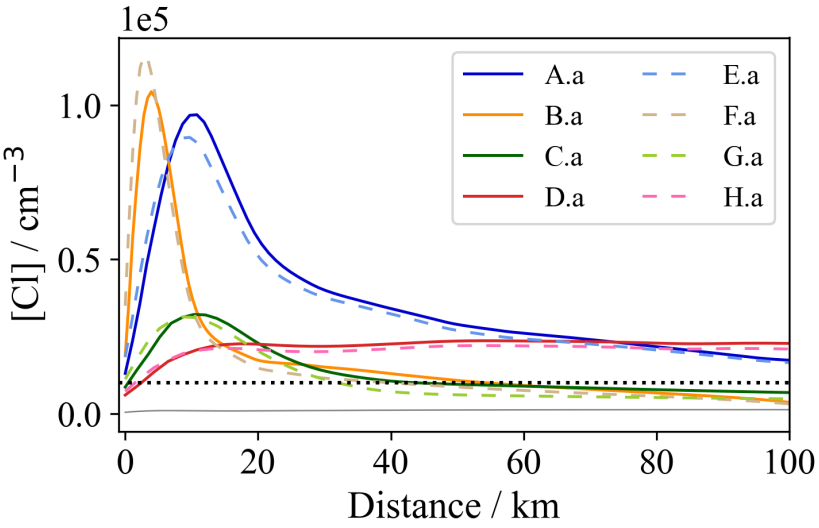

Figure 2. Cl concentrations for an Fe emission of 0.021 g/s for all dispersion scenarios. The background concentration is the fully drawn grey line and the detection limit, 1×10^4 cm^{-3}, is the dotted black line. Dashed lines indicate tower emissions and full lines are used for ship emissions. Similar colors indicate similar dispersion scenarios.

3.3 Cl_2

Background Cl_2 levels in our model were always below 1 ppt, and the addition of even small amounts of ISA leads to peak Cl_2 concentrations of above 10 ppt that are clearly above the detection limit of 2 ppt (see Figure 3, showing emission scenario a for all dispersion scenarios). Ship and tower emissions result in similar Cl_2 concentrations for the same dispersion scenarios.

The peak of Cl_2 occurs within 5 km of the emission source.

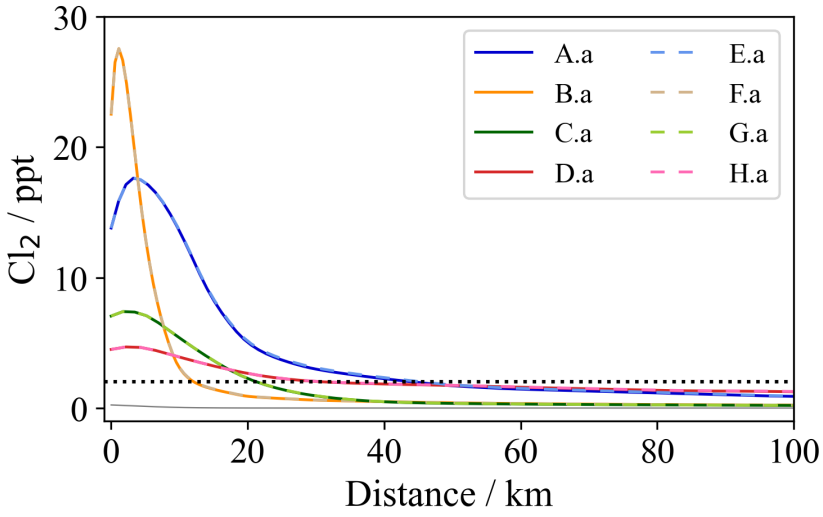

Figure 3. Cl_2 concentrations for a Fe emission of 0.021 g/s for all dispersion scenarios. The background concentration is the fully drawn grey line and the detection limit, 2 ppt, is the dotted black line. Dashed lines indicate tower emissions and full lines are used for ship emissions. Similar colors indicate similar dispersion scenarios.

3.4 ClO

Figure 4 shows the model output for ClO. The high NO_x levels in ship plumes (scenarios A-D) strongly reduce ClO, through the reaction ClO + NO_2 that forms $ClNO_3$. Further away from the ship NO_x levels are lower, leading to an increase in ClO, but for low and medium iron emission scenarios this still does not generate enough ClO to exceed the detection limit of 5 ppt. Because of this, high iron emissions of 2 g/s are needed at the source, to generate a signal that can be detected (see Figure 4, showing the highest emission scenario c for ship scenarios A-D with solid lines). We conclude that measurements of ISA based on perturbation of ClO in a ship plume are not practical unless the NO_x emissions of the ship are eliminated, or if a high amount of additional Fe is added to the plume.

The situation is very different for the scenarios with pure iron emissions without NO_x (scenarios E-H), see Figure 4, showing the medium emission scenario b for tower scenarios E-F with dashed lines. In these scenarios, a high ClO signal (above 10 ppt) is found up to at least 50 km from the ship, and should be measurable with a medium Fe emission rate (0.2 g/s). The peak ClO signal occurs close to the emission tower, between 4-10 km for most scenarios.

Scenarios A and E have a relatively high ClO signal compared to the other scenarios, because scenario A and E have more pristine background air conditions with a lower NO_x background of 7 ppb, compared to 50 ppt in the other scenarios.

To be able to compare our results with Song et al. (2003), we used relatively low ozone background levels that are still typical for the remote marine boundary layer. A higher ozone background could slightly increase ClO concentrations, but not to an extent that it changes the conclusions substantially.

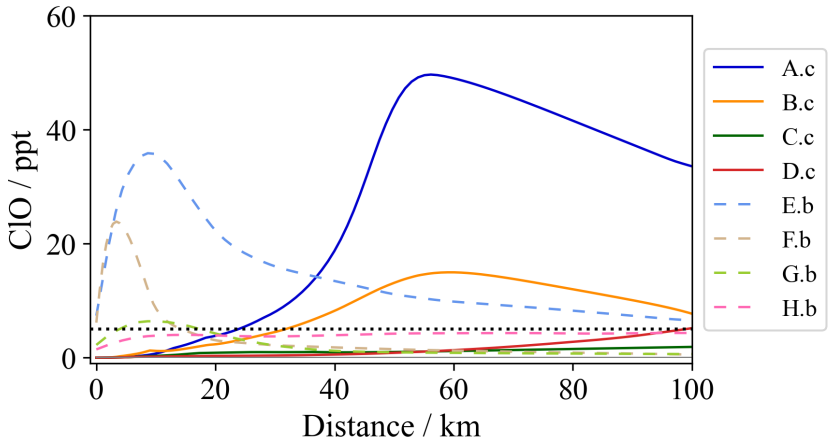

Figure 4. ClO model output for a sunrise emission in all dispersion scenarios and using the highest emission scenario c for ships (solid lines) and a medium emission scenario b for towers (dashed lines). The background concentration is the fully drawn grey line and the detection limit, 5 ppt, is the dotted black line. Similar colors indicate similar dispersion scenarios.

3.5 HOCl

While HOCl is formed in a ship plume via the reaction of OH with species such as $ClNO_3$, $ClNO_2$ and Cl_2, the main source is $ClO + HO_2$. Due to NO_x depleting O_3 (see Table 3), both HO_x and ClO are depleted close to the ship, which explains why HOCl levels only increase several tens of km from the ship, more or less in tandem with the ClO concentration profile (see Figure 5, showing the highest emission scenario c for all dispersion scenarios). The far distance from the emission point creates challenges for its detection, both from a logistical perspective, as well as by increasing the dependence on meteorology. For a tower emission (without NO_x, see dotted lines in Figure 5) the HOCl concentrations increase immediately, because the ClO and HO_x are not depleted close to the emission source.

The HOCl background concentration in our model output is always below 1 ppt, also for ships without Fe emissions. For ships, the emission of 0.021 - 0.2 g/s Fe is not sufficient to raise the HOCl concentration above the detection limit of 30 ppt, while for towers 0.2 g/s results in HOCl concentrations close to the detection limit. For 2 g/s Fe emissions, our model predicts a strong HOCl concentration that can still be detected far away from the emission source (100 km or more).

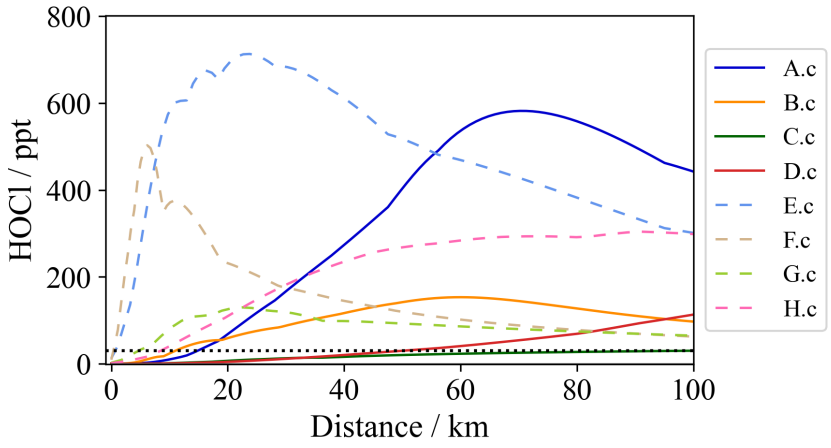

Figure 5. HOCl model output for a sunrise emission, using the highest emission scenario c for all dispersion scenarios. The background concentration is the fully drawn grey line and the detection limit, 30 ppt, is the dotted black line. Dashed lines indicate tower emissions and full lines are used for ship emissions. Similar colors indicate similar dispersion scenarios.

3.6 $ClNO_3$

Figure 6 shows the model output for $ClNO_3$, showing a medium emission scenario for all dispersion scenarios. $ClNO_3$ takes a long time to form (compared to other species investigated in this study), because it is formed from ClO + NO_2 in a three-body reaction. It also has a long lifetime in the atmosphere of hours to days, depending on hydrolysis rate(Pennacchio, van Herpen, et al., 2024)). This leads to a buildup of concentration with distance. Typically, $ClNO_3$ starts to rise 10 km from the source (in tandem with increases in ClO), and peaks beyond 40 km.

At high distance, NO_x emissions from other ships could slightly increase the $ClNO_3$ levels, but the $ClNO_3$ could then still be attributed to the ship emitting the $FeCl_3$ as that is the limiting factor.

Despite low NO_x background levels, the $ClNO_3$ concentrations in a tower emission plume without NO_x are of the same order of magnitude as in ship plumes. This can be explained by the long distance at which $ClNO_3$ starts to form, at which point the NO_x levels in the ship plume have already dispersed into the background.

For the lowest Fe emission scenario, the $ClNO_3$ concentration is just below the detection limit of 3 ppt. An emission of 0.21 g/s leads to a clear $ClNO_3$ signal that can be detected far from the source.

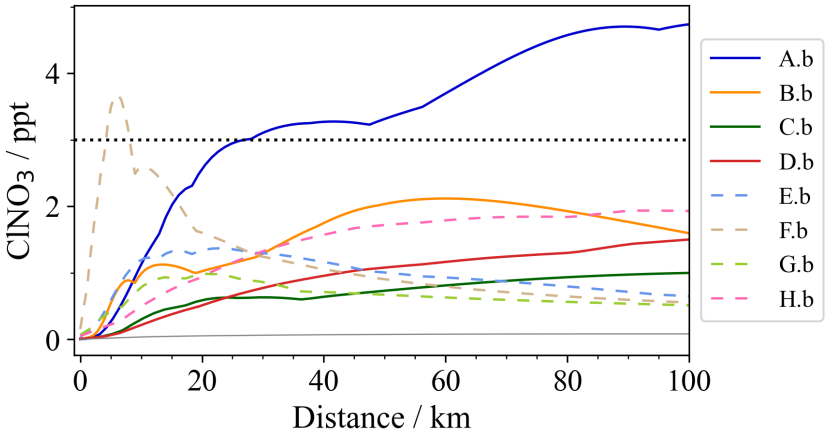

Figure 6. Model output for $ClNO_3$ for a sunrise emission, in a medium emission scenario for all dispersion scenarios. The background concentration is the fully drawn grey line and the detection limit, 3 ppt, is the dotted black line. Dashed lines indicate tower emissions and full lines are used for ship emissions. Similar colors indicate similar dispersion scenarios.

3.7 $ClNO_2$

Figure 7 shows the model output for $ClNO_2$, for a medium emission scenario and with separate panels for ships and towers, because the concentrations are very different. $ClNO_2$ forms rapidly from the reaction of Cl + NO_2 and has a relatively short lifetime, resulting in a peak concentration close to the emission source (6 - 12 km). $ClNO_2$ gives a very strong signal for ship plumes due to the NO_x emission by the ship, requiring an iron emission of 0.21 g/s to exceed the detection limit of 10 ppt. However, for tower emissions the NO_x levels are too low to generate a significant $ClNO_2$ signal for any of our emission scenarios. Thus, $ClNO_2$ is only useful in field tests where NO_x is emitted along with the iron.

An important additional factor when using $ClNO_2$ is that it is important to also track variations in the background $ClNO_2$ concentration, especially in the morning when $ClNO_2$ that formed during the night (from N_2O_5 uptake on sea salt aerosol) will rapidly photolyze.

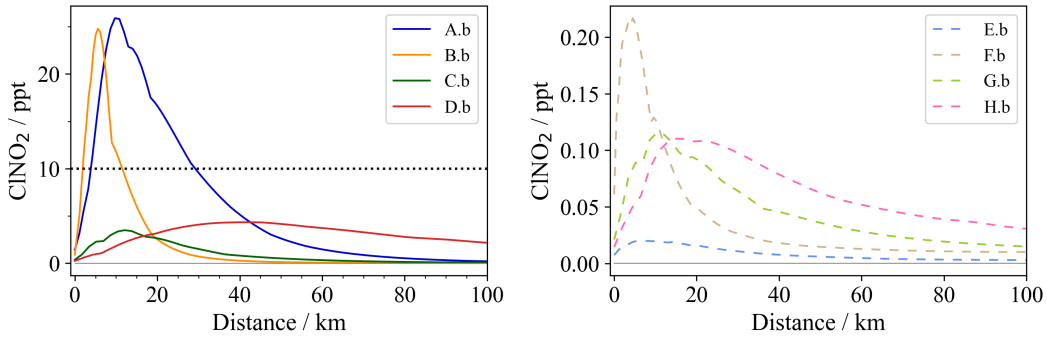

Figure 7. Model output for $ClNO_2$ for a sunrise medium emission scenario. Left: ship scenarios A-D. Right: tower scenarios E-F. The background concentration is the fully drawn grey line and the detection limit, 10 ppt, is the dotted black line. Similar colors indicate similar dispersion scenarios.

3.8 CO:ethane ratio

Figure 8 shows how the CO:ethane ratio develops in a ship plume compared to the background air, for a medium emission scenario B.b. While we start our simulation with an CO:ethane background ratio of 200, this ratio changes during the stabilization of the model (before iron emission) due to background Cl levels, resulting in a background CO:ethane ratio at the start of the iron emission of around 400 for scenario B (see Figure 8). Initially the emission of CO and ethane with a ratio of 50 leads to an increase in both CO and ethane, but the ethane levels are increased relatively more, pushing the CO:ethane ratio down towards 50. Within the first 10 km the CO concentration in the ship plume drops to the ambient level, while the ethane concentration continues to decrease, eventually to below background air concentrations. This becomes detectable when the CO:ethane ratio increases to a value above the background level, giving evidence of increased Cl.

The sensitivity of this method depends on the accuracy of the ethane measurement (10 ppt). In scenario B, at 100 km we find an ethane concentration of 210 ppt without iron emissions, while the background concentration is 212 ppt. Thus, without iron emissions there is a slight reduction in ethane due to the increased Cl concentrations due to the NO_x emission. An iron emission of 0.2 g/s is needed to sufficiently reduce ethane for detection, at 100 km distance leading to ethane inside the ship plume of 196 ppt (14 ppt reduction) (see Figure 8).

For a background CO:ethane ratio of 300 to 400, using a 10 ppt accuracy for the ethane measurement, the method is sensitive to changes of at least 10 - 20 in the CO:ethane ratio. If the background CO:ethane ratio is lower, the method will be more sensitive. Figure 9 shows the changes in CO:ethane ratio for the various scenarios, with a medium iron emission of 0.2 g/s.

As can be seen in Figure 9, the CO:ethane ratio is easier to interpret for tower emissions without NO_x, mainly because these scenarios do not emit CO and ethane from the emissions source. Because of this, any Cl that is generated will immediately lead to an increase of CO:ethane above the background, allowing the method to work closer to the emission source. However, the amount of Fe needed for a clear signal is the same for both ship and tower emissions. Also, because tower emissions will not emit ethane, the background ethane concentration may in some cases be too low to be detectable.

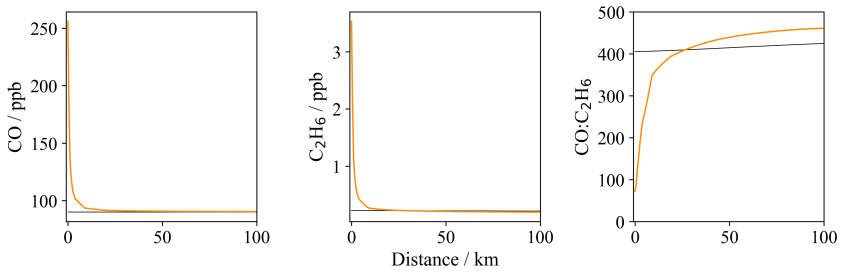

Figure 8. Illustration of CO and ethane changes for a medium ship emission in scenario B.b. The background values are the fully drawn black lines.

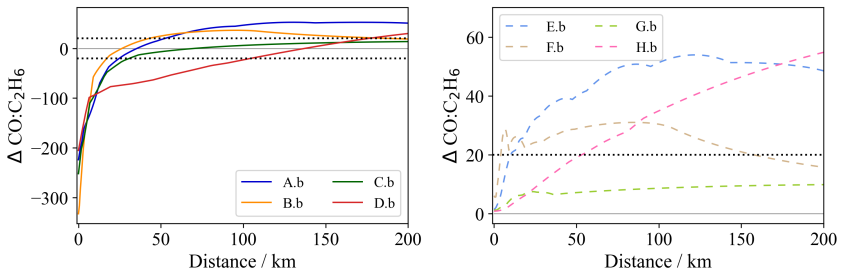

Figure 9. Model output for CO:ethane ratio for a sunrise medium emission scenario for all dispersion scenarios. Left: ship scenarios A-D. Right: tower scenarios E-F. The background values are the fully drawn grey line and the detection limit, ±20, is the dotted black line. Similar colors indicate similar dispersion scenarios.

3.9 δ^{13}C(CO)

Figure 10 shows the modeled δ^{13}C(CO) for each scenario, using a high iron emission. It is important to note that the highest Fe emission scenario c (i.e. 2.1 g/s) is the only scenario which produces an isotopic shift large enough for statistically significant detection by the analytical system (greater than 0.2 ‰ in δ^{13}C(CO)). The CO isotopic composition changes most strongly within 20 km of the iron source, consistent with maximum Cl concentrations in Figure 2. For ship emission scenarios (i.e. A-D), an initial isotopic enrichment occurs due to the addition of isotopically heavy CO (δ^{13}C = -25 ‰), relative to the background (δ^{13}C = -30 ‰). For this reason, isotopic depletions below background δ^{13}C(CO) due to chlorine oxidation are not detectable until 5, 10, 15 and 20 km from the emission source for scenarios A, B, C and D, respectively. For all scenarios, the total magnitude of depletions below background δ^{13}C(CO) ranges from 0.4 – 2.0 ‰ within 60 km.

From these results, the primary obstacle in using δ^{13}C(CO) as a detection method for enhanced Cl oxidation in ship plumes is the slow reaction rate of the Cl + CH_4 reaction. Flask samples must be obtained from air that has been sufficiently processed to reflect the CO signature of chlorine oxidation, rather than the combusted fuel source. The model also assumes zero interference from intersecting plumes. In a field study, intersecting plumes should be avoided or reduced when determining sample locations. If this not possible, additional corrections are necessary for data interpretation.

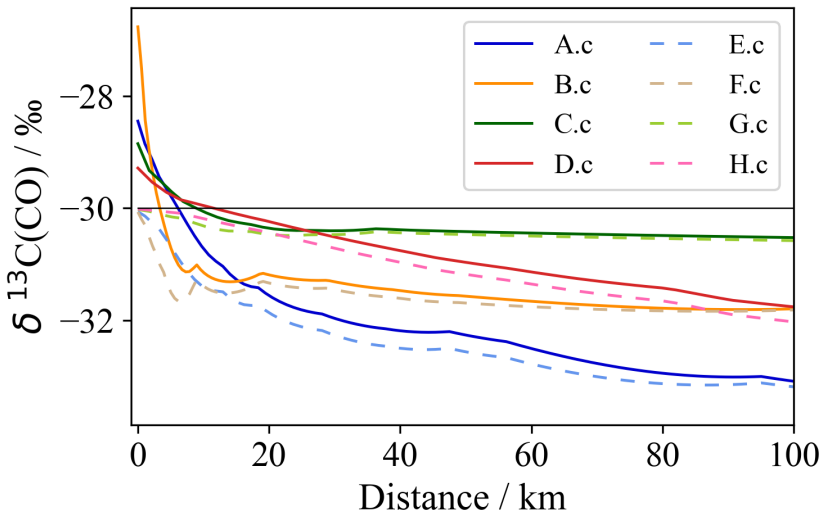

Figure 10. Plume model output for CO isotope changes for a sunrise emission for high Fe emission in all dispersion scenarios. The background value is the fully drawn black line and the detection limit is ± 0.2 ‰. Dashed lines indicate tower emissions and full lines are used for ship emissions. Similar colors indicate similar dispersion scenarios.

3.10 CH_2O

To show the impact of iron emissions on HCHO in the plume, Figure 11 shows our model output for CH_2O for varying iron emissions in scenario A and E. The baseline result for scenario A.0 without Fe emission is in agreement with similar scenarios that were modeled by Song et al. (2010). There is an initial small drop in CH_2O during the initial phase of O_3 and OH depletion close to the ship. This is followed by an increase in CH_2O concentrations when O_3 and OH recover above the background leading to increased CH_4 oxidation that leads to CH_2O formation. Our model does not include CH_2O emissions by the ship itself, but Song et al. (2010) showed that these emissions only have a minor influence on the CH_2O concentrations in the ship plume. Our model also does not include non-methane VOCs that could be a potential source for photochemical HCHO production. This does not affect our conclusions on the useability of HCHO, because Song et al. (2010) found that NMVOC emissions from ships were not a primary source of photochemical HCHO production inside ship plumes due to their rapid and individual dilution.

In appendix Figure *A*1 it can be seen that in scenario A.c (the highest iron emission for the scenario comparable to Song et al. (2010)) the maximum concentration of Cl occurs closer to the ship than for OH. This is because the Cl production from emitted iron is not affected by the initial O_3 depletion (while OH is depleted due to this). This is why the iron emissions increase CH_2O concentrations close to the ship. With high Fe emissions, this leads to a double peak in CH_2O concentrations; the first one from the Fe induced Cl emission (around 10-30 km distance in this scenario) and a second peak from the OH chemistry in the plume (around 60-80 km distance). The strength of the CH_2O signal is above the 100 ppt detection limit for iron emissions of 0.21 g/s, but there is no clear difference in the shape of the CH_2O curve, requiring a reference measurement without Fe emission. A challenge is that in practice, a reference measurement without Fe emission may not be available. In that case, the Cl emission can be detected only when there is a clear double-peak, which requires high Fe emissions of 2.1 g/s. In addition, because the HCHO peak resulting from Cl oxidation occurs close to the ship, MAX-DOAS

detection will be complicated due to high aerosol levels in the plume, which will negatively affect the detection limit, again requiring higher Fe emissions to be detectable. Alternatively, a second species that is more closely related to the OH chemistry might be measured, for example HNO_3 formed from NO_2 + OH, or H_2SO_4 formed by the OH initiated oxidation of SO_2 (Kim et al., 2013). For example, in our model output HNO_3 peaks at approximately the same distance from the ship as OH (see Appendix A, Figure A1), so if CH_2O peaks earlier than HNO_3, that could indicate Cl production by Fe in the ship plume. For HNO_3 such a measurement is challenging in view of detection limits, but for H_2SO_4 this would be feasible with a chemical ionization mass spectrometer (CIMS) mounted on an aircraft (G. Chen et al., 2005).

For Fe emission without NO_x, the CH_2O signal from Cl oxidation of methane is more clearly visible, because there is no OH peak from the NO_x emission (so there is also no double-peak, only one peak from Cl). This means that no reference measurement is needed for the interpretation by a tower without NO_x.

Figure 12 show the model output for the different dispersion scenarios. Without a reference measurement, CH_2O would be an attractive indicator for Cl production, but it needs an iron emission of 2.1 g/s in shipping plumes, and 0.21 g/s in tower emissions. A reference measurement of for example H_2SO_4 can reduce the minimum iron emission for ship plumes to 0.21 g/s. /hlIt is important to also track background HCHO concentrations during a field study, because HCHO in background air will vary through the day due to fluctuations in VOC oxidation, or due to fluctuations in continental sources.

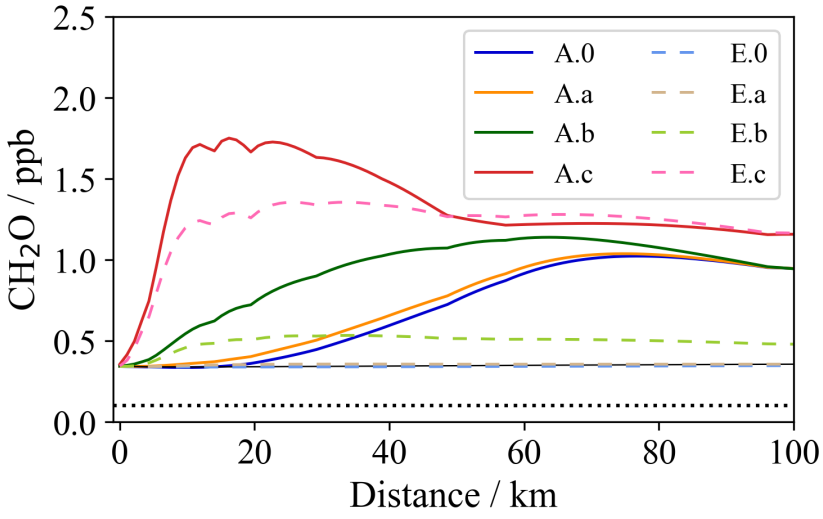

Figure 11. Plume model output for CH_2O along the center line of the ship plume for similar dispersion scenarios A (for ships, full lines) and E (for towers, dashed lines) and for varying Fe emissions, showing how the CH_2O levels change with increasing Fe emission (see Table 1). The background concentration is the fully drawn grey line and the detection limit, 0.1 ppb, is the dotted black line. Similar colors indicate similar Fe emission scenarios.

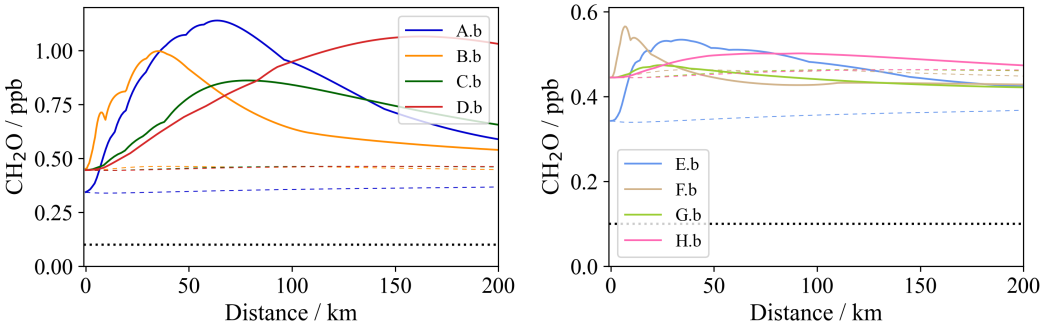

Figure 12. Plume model output for CH_2O for a medium sunrise emission scenario in all dispersion scenarios. Left: ship scenarios A-D. Right: tower scenarios E-F. The fully drawn lines are for the various scenarios, and the dashed lines are the corresponding background concentrations. The detection limit, 0.1 ppb, is the dotted black line

3.11 Other species

While the ultimate benefit for iron-salt aerosol emissions would be methane and ozone removal, both species were not found to be helpful indicators for the removal, because the background concentrations are too high compared to the removal amount.

In the case of methane, the additional OH chemistry in the ship plume leads to a methane reduction in our model output of 1 ppb within the plume, while the Cl chemistry from the lowest emission scenario removes only 0.1 ppb of additional methane, and for the highest emission scenario of 2.1 g/s the methane reduction in the plume is still only 3 ppb at a background of 1.8 ppm. This is too low to detect in a real world field test, where methane will naturally vary due to varying local sources.

For ozone, the impact of the additional Cl chemistry is that the first plume phase of ozone depletion and recovery is accelerated, leading to an ozone recovery closer to the ship. However, the shape and peak of the ozone concentration profile remains the same, making it very hard to demonstrate the impact of the Cl chemistry, unless a direct comparison can be made with and without the iron emissions.

3.12 Overview of results

Table 4 and Table 5 provide an overview of the minimum Fe emission required to detect Cl production by the iron in a NO_x polluted ship plume and in a clean iron plume. For an overview of the signal strength for each Fe emission scenario, we refer to Appendix B, Table B1.

Table 4. Overview of minimum Fe emission needed for detectable signal above limit of detection (LOD) for ship plume emissions including NO_x/CO/ethane, showing the range of signals across all scenarios based on the difference between ambient background and baseline without iron emission.

Species	**Background**	**Baseline**	**Fe / g s^{-1}**	**Signal**	**Dist. / km**	**LoD**[e]
Fe[f]	0 - 10 ng/m^3	0	0.021	1 - 100 ng/m^3	1 - 60	1 ng/m^3
Cl	$< 10^4$/cm^3	$< 10^4$/cm^3	0.021	2-10 10^4/cm^3	4-20	1 10^4/cm^3
Cl_2	<1 ppt	<1 ppt	0.021	5-25 ppt	1-4	2 ppt
$ClNO_3$	<1 ppt	<1 ppt	0.21	5 - 45 ppt	>20	3 ppt
$ClNO_2$	<1 ppt	<1 ppt	0.21	5 - 25 ppt	6 - 12	10 ppt
CO:C_2H_6[a]	NA	4	0.21	0 - 60	100	20
ClO	<1 ppt	<1 ppt	2.1	3 - 50 ppt	60	5 ppt
HOCl	< 1 ppt	<1 ppt	2.1	35 - 580 ppt	60-200	30 ppt
δ^{13}C(CO)[b]	NA	<0.1 ‰	2.1	0.6 - 3 ‰	100-400	0.2 ‰
CH_2O[c]	NA	660 ppt	2.1	1360 ppt	10-30	100 ppt[d]

[a] Delta with background; mole/mole.
[b] Depletion in δ^{13}C(CO) relative to background.
[c] Delta with background; mole/mole.
[d] With reference measurement, or 1000 ppt without reference.
[e] Limits of detection: Photoactive Fe (X. R. Zhu et al., 1997; Y. Chen & Siefert, 2003), Cl (Baker et al., 2011, 2016), Cl_2 (Lawler et al., 2011), ClO (Stutz et al., 2002), HOCl (Lawler et al., 2011), $ClNO_3$ (Marcy et al., 2005), CO:C_2H_6 (Read et al., 2009), CH_2O (Plane & Saiz-Lopez, 2006; Prados-Roman et al., 2020), δ^{13}C(CO)[b] (Pathirana et al., 2015), $ClNO_2$ (von Clarmann & Johansson, 2018).
[f] Photoactive Fe

Table 5. Overview of minimum Fe emission needed for detectable signal above limit of detection (LOD) for tower emissions without NO_x/CO/ethane, showing the range of signals across all scenarios based on the difference between ambient background and baseline without iron emission.

Species	Background	Baseline	Fe / g s^{-1}	Signal	Dist. / km	LoD[e]
Fe[f]	0 - 10 ng/m^3	0	0.021	1 - 100 ng/m^3	1 - 60	1 ng/m^3
Cl	< 10^4/cm^3	<10^4/cm^3	0.021	2-10 10^4/cm^3	4-20	1 10^4/cm^3
Cl_2	<1 ppt	<1 ppt	0.021	5-25 ppt	1-4	2 ppt
ClO	<1 ppt	<1 ppt	0.21	4 - 36 ppt	3 - 10	5 ppt
HOCl	<1 ppt	<1 ppt	0.21	10 - 90 ppt	7 - 25	30 ppt
$ClNO_3$	<1 ppt	<1 ppt	0.21	5 - 22 ppt	>7	3 ppt
CO:C_2H_6[a]	NA	0	0.21	10 - 50	100	20
CH_2O[c]	NA	0	0.21	190 ppt	20	100 ppt
$\delta^{13}C(CO)$[b]	NA	<0.5 ‰	2.1	0.6 - 3 ‰	100 - 400	0.2 ‰
$ClNO_2$	<1 ppt	<1 ppt	>2.1	<1 ppt	NA	10 ppt

[a] Delta with background; mole/mole.
[b] Depletion in $\delta^{13}C(CO)$ relative to background.
[c] Delta with background; mole/mole.
[e] Limits of detection: Photoactive Fe (X. R. Zhu et al., 1997; Y. Chen & Siefert, 2003), Cl (Baker et al., 2011, 2016), Cl_2 (Lawler et al., 2011), ClO (Stutz et al., 2002), HOCl (Lawler et al., 2011), $ClNO_3$ (Marcy et al., 2005), CO:C_2H_6 (Read et al., 2009), CH_2O (Plane & Saiz-Lopez, 2006; Prados-Roman et al., 2020), $\delta^{13}C(CO)^b$ (Pathirana et al., 2015), $ClNO_2$ (von Clarmann & Johansson, 2018).
[f] Photoactive Fe.

4 Discussion

Here we studied the release of $FeCl_3$ into ship plumes instead of ISA particles forming via iron in shipping fuels. There are reasons to believe that the emission of $FeCl_3$ for the purpose of removing methane could be cost-effective, and that compared to iron from shipping combustion, direct $FeCl_3$ emissions are likely to be more efficient, while having less uncertainties. van Herpen et al. (2023) reported the removal of 7.5 g of CH_4 per g of photoactive iron in North Atlantic mineral dust/sea spray aerosols per day, with approximately 2% of iron in mineral dust being photo-active. Assuming that a shipping fuel additive such as ferrocene (ca. 117$ per kg Fe (Chemistry, 2024), see Table 6) also results in 2% photo-active iron (which is a pessimistic assumption, because shipping iron emissions are expected to have relatively high solubility (Ito, 2013)), and assuming a 5 day particle lifetime, leads to a best-case cost-efficiency of $ 4,300 - 5,500 per ton CO_2e. However, researchers have also proposed to inject $FeCl_3$ into shipping plumes or spray it from ocean towers (Oeste et al., 2017; Ming et al., 2021), which implies 100% photoactive iron (50× improvement), and $FeCl_3$ is 40× cheaper than ferrocene ($3 per kg Fe), and could therefore bring costs down to levels below what is currently expected for atmospheric CO_2 capture technologies (below $10 per Mg(metric ton) of CO_2e).

Table 6. Estimated cost of ISA technologies

Method	Cost (USD / kg(Fe))	Chemical form	Name	Cost of equipment
Spray $FeCl_3$ aerosols	~ 1	$FeCl_3$	Iron chloride	N/A[a]
	~ 3	Fe	Elemental iron	
Add iron to shipping fuel	~ 35	$Fe(C_5H_5)_2$	Ferrocene	~ 0[b]
	~ 117	Fe	Elemental iron	~ 0[b]

[a] Estimates not available.
[b] No additional equipment needed as iron is present as additive in fuel.

These are best-case cost estimates where global modeling of mineral dust showed that CH_4 was only removed efficiently above certain parts of the ocean, due to loss of O_3 and OH resulting in increasing CH_4 lifetime (van Herpen et al., 2023). Pennacchio, van Herpen, et al. (2024) used box modeling to show that low intensity Cl generation, such as by iron in a dispersed shipping plume, only decreases CH_4 lifetime for very low or very high background NO_x concentrations (the precursor for O_3). Because of this, conditions in most of the Northern Hemisphere, and for most shipping routes, are unfavorable. Meidan et al. (2024) used global modeling to show that a threshold amount of combustion iron emissions from shipping are needed before removal of CH_4 starts to occur. Based on the assumption that the fraction of photoactive iron in the combustion emissions is low, the paper finds that direct radiative forcing by the iron can cancel cooling from the reduction in CH_4 and O_3. At the same time, the indirect cooling from the iron via for example cloud effects is potentially larger than the direct warming effect, but is highly uncertain. If emitted iron is fully photo-active, these concerns and uncertainties about iron radiative forcing are strongly reduced, as 50× less material would be needed.

Sulfate aerosol chemistry is reported to partly inhibit chlorine production from iron salt aerosols (Wittmer, Bleicher, & Zetzsch, 2015; Wittmer, Bleicher, Ofner, & Zetzsch, 2015; Mikkelsen et al., 2024). To account for sulphate chemistry in our model, we would need to include aqueous chemistry that accounts for the interaction between Fe(II) and SO_4^{2-} in the aerosol phase, which is beyond the scope of this study. Wittmer measured in a smog chamber that the addition of 200 ppb SO2 decreased the Cl2 production by 30%. However, much lower SO_2 concentrations of up to 1 ppb have been measured in ship plumes (G. Chen et al. (2005)). According to Mikkelsen et al. (2024) aerosol sulfur chemistry will form iron sulfate complexes and partly inhibit the available iron for the ISA mechanism. When modeling by Mikkelsen et al. (2024) included an aerosol mass fraction of 50% $SO_4^{2}-$, which is 10 times the fraction of sea spray aerosols, it reduced the formation of iron(III) chlorides by up to 40%. For high-sulfur fuels (above 0.5% sulfur), up to 50% $SO_4^{2}-$ mass fraction was observed in particulate matter (Lack et al., 2009)), but our study focuses on contemporary fuels with less than 0.5% sulfur (compliant with new IMO sulfur regulations), which have orders of magnitude lower $SO_4^{2}-$ fraction. Thus, even in a high-sulfur scenario the reduction in Cl_2 production might be up to 40%. This uncertainty is low in view of the uncertainty in the cycling rate for Cl_2 production (6 to 78 per hour), which means the added uncertainty of excluding aerosol sulfate chemistry in our model is negligible.

Based on our analysis, the detection of photo-active iron appears to be the most sensitive approach to quantify the ISA chemistry, because it detects iron-salt aerosols directly. It can be used for a wide range of distances, and even very low iron-salt aerosol emissions are already detectable. However, this method does not detect Cl production

by these aerosols, so it is not a suitable method for a field test that studies the impact of the Cl emissions.

There is a range of species that could detect Cl production from relatively low Fe emissions and can be detected with CIMS. From the species we analyzed, Cl_2 appears the most sensitive to the Fe emissions and in a field study it may be most practical species to measure, because according to the model the peak in Cl_2 concentration would result close to the emission point, which is a logistical advantage compared to some of the other species that have their concentration peak tens of km downwind, making those observations more meteorology-dependent.

For NO_x-polluted ship plumes, CIMS could also be used for $ClNO_3$, $ClNO_2$, and to a lesser extent ClO and HOCl. CIMS detection of HOCl and ClO works better for iron emissions without NO_x, while $ClNO_2$ is not detectable at all without NO_x emissions accompanying the iron-salt aerosols. While the radical clock method for Cl detection appears highly sensitive, we believe the applicability of this approach is limited due to the entrainment of background air into the plume. However, we show for a radical clock with CO and ethane that it is possible to account for this when the radical clock leverages background air species.

While the use of CIMS seems the most suitable for low Fe emissions, a field study might not be limited by the available Fe emission, making simpler and lower-cost techniques available. Sturtz's environmental impact study (Sturtz et al., 2022) investigated Fe emissions up to 0.21 g/s and identified no significant impacts. Further impact studies are needed to show whether our highest scenario of 2.1 g/s would be safe for a field study.

For high Fe emissions of 0.21 g/s and above, the ratio of CO:ethane has the advantage that low-cost spectroscopic methods could be used to generate real-time and high-resolution data that is closely related to Cl chemistry. The use of flask measurements for analysis of $\delta^{13}C(CO)$ has the great advantage that it gives a direct quantification of the amount of methane removed by Cl. DOAS methods are also possible with high Fe emissions. For example, MAX-DOAS could be used to measure the double-peak of CH_2O along the center line, or at very high Fe emissions even satellite detection might be possible. With LP-DOAS a ClO signal could be measured for a high Fe emission, especially for Fe emissions without NO_x.

This study did not investigate the influence of anthropogenic emissions on natural mineral dust/salt aerosols (van Herpen et al., 2023). Anthropogenic pollution can increase the acidity of particles which is likely to increase the release of iron from mineral particles by weathering and will shift aqueous equilibria towards the formation of iron-chloride chromophores, overall increasing Cl production and methane removal. In addition, anthropogenic NO_x emissions into mineral dust clouds can shift the secondary atmospheric chemistry into conditions favorable for methane removal (Pennacchio, van Herpen, et al., 2024).

Pennacchio, van Herpen, et al. (2024) showed that high Cl_2 emissions of above $1{\times}10^6$ Cl_2 /(cm^3 s) always leads to a net decrease of methane's lifetime, and that lower Cl_2 emissions can lead to a methane lifetime increase for specific NO_x conditions. A question is what Fe emission is needed for the Cl_2 production to remain above 1×10^6 Cl_2 /(cm^3 s), even for a fully dispersed plume. Bearing in mind that multi-day plume modeling is better done in a global model that includes meteorology, we still examined our model output for an initial estimate. For our most stable plume scenario A, our highest Fe emission of 2 g/s resulted in Cl_2 production of $1{\times}10^4$ Cl_2 /(cm^3 s) with peak sunlight conditions after 5 days of dispersion. This suggests that more than 100× higher Fe emission is needed (above 200 g/s) to remain in the high ClO_x regime during the entire dispersion of the plume. A question is whether such high Fe emissions and associated Cl_2

emissions are practical in view of environmental impact and in view of CH_4 depletion within the ship plume.

5 Conclusion

Considering the urgency of addressing atmospheric methane concentrations to limit global warming (Gorham et al., 2024), while natural methane emissions are on the rise (Lan et al., 2024), there could be a role for the application of iron-salt aerosol as methane removal technology, if it is proven safe and effective, and if effective governance is in place. Safety and efficiency questions will require field studies that quantify Cl production from iron-salt aerosol emissions. Because ISA emissions can also lead to methane lifetime increase (Pennacchio, van Herpen, et al., 2024; van Herpen et al., 2023; Meidan et al., 2024; Li et al., 2023), quantification methods could also support governance.

We identified several potential techniques to quantify Cl production by ISA in plumes, ranging from CIMS detection (of $ClNO_3$, HOCl, ClO, $ClNO_2$), spectroscopic detection of CO:ethane ratio, DOAS detection of CH_2O and ClO and isotopic analysis of $\delta^{13}C(CO)$.

The hypothetical field study for which Sturtz et al. (2022) performed an environmental impact analysis, could demonstrate Cl production from $FeCl_3$ emissions using the relatively simple method of measuring CO:ethane ratio from a fixed position, or measuring the amount of photoactive iron in the plume, but most likely will need to use a CIMS to detect species like Cl_2, $ClNO_3$ and $ClNO_2$. DOAS is not likely to work for this field study. Alternatively, the environmental impact analysis should be done for $10\times$ higher Fe emissions, so that other more low-cost techniques can be employed.

Appendix A Sunrise emission in scenario A.b

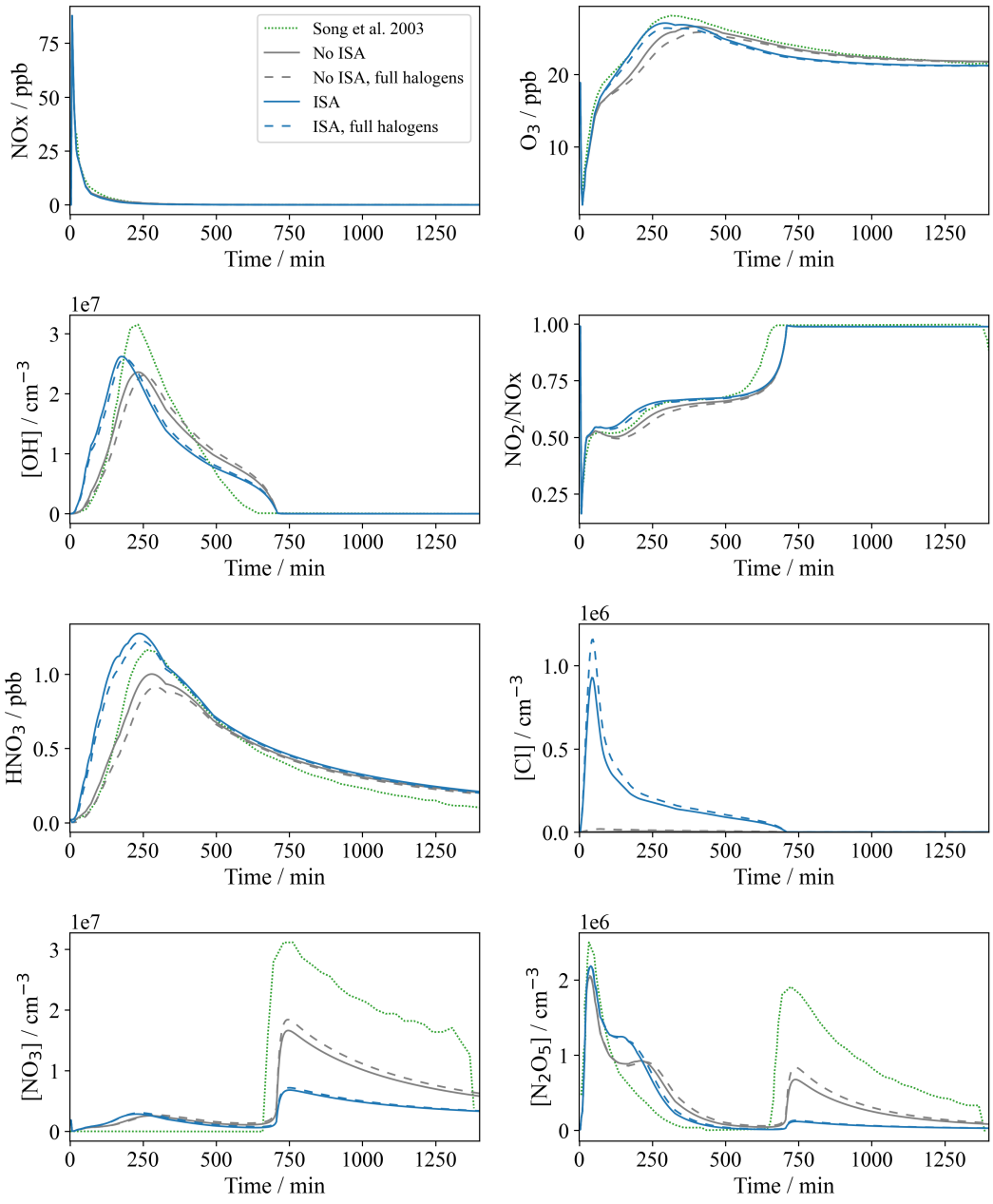

Figure A1. Ship plume model output for several species for a sunrise emission in scenario A.0 (labeled "No ISA" for the scenario without iron-salt aerosols, and A.b "ISA" for the medium Fe emission of 0.21 g/s emission), in comparison with the Song et al. (2010) results for a similar scenario, showing good agreement between the models. Differences are attributed mainly to differences in the dispersion rate of the plume and the addition of Cl chemistry into our model. Dashed lines show the results of a sensitivity analysis when including iodine and bromine chemistry in addition to chlorine chemistry (labeled 'full halogens')

Appendix B Peak values and LoD

Table B1. Peak values of Fe, Cl, Cl_2, ClO, HOCl, $ClNO_3$, $ClNO_2$, $\Delta CO:C_2H_6$, $\delta^{13}C(CO)$ and CH_2O at various Fe emission rates (Fe_E) compared to limit of detection (LoD) for each compound. Distance is given in km and peak values above the LoD is marked in green.

	Ship		Tower		Ship		Tower	
Fe_E / g s^{-1}	Fe / ng m^{-3}	Dist.	Fe / ng m^{-3}	Dist.	Cl / cm^{-3}	Dist.	Cl / cm^{-3}	Dist.
Bkgd	0-10		0-10		$<1\times10^4$		$<1\times10^4$	
0	0		0		$<1\times10^4$		$<1\times10^4$	
0.021	1 - 100	1-60	1 - 100	1-4	2×10^4 - 1×10^5	4-20	2×10^4 - 1×10^5	4 - 20
0.21	10 - 1000	>1	10 - 1000	>1	2×10^5 - 1×10^6	4-20	2×10^5 - 1×10^6	4 - 20
2.1	1000 - 10000	>1	1000 - 10000	>1	2×10^6 - 9×10^6	4-20	2×10^6 - 9×10^6	4 - 20
LoD	1		1		1×10^4		1×10^4	

	Ship		Tower		Ship		Tower	
Fe_E / g s^{-1}	Cl_2 / ppt	Dist.	Cl_2 / ppt	Dist.	ClO / ppt	Dist.	ClO / ppt	Dist.
Bkgd	<1		<1		<1		<1	
0	<1		<1		<1		<1	
0.021	5 - 25	1-4	5 - 25	1-4	<1	>80	0.4 - 5	2 - 9
0.21	50 - 250	1-4	50 - 250	1-4	<1.6	>80	4 - 36	3 - 10
2.1	500 - 2500	1-4	500 - 2500	1-4	3 - 50	60	40 - 110	3 - 10
LoD	2		2		5		5	

	Ship		Tower		Ship		Tower	
Fe_E / g s^{-1}	HOCl / ppt	Dist.	HOCl / ppt	Dist.	$ClNO_3$ / ppt	Dist.	$ClNO_3$ / ppt	Dist.
Bkgd	<1		<1		<1		<1	
0	<1		<1		<1		<1	
0.021	3 - 8	130 - 400	1 -10	7 - 100	2 - 5	>20	1 - 3.5	>7
0.21	3 - 26	130 - 400	10 - 90	7 - 25	5 - 45	>20	5 - 22	>7
2.1	35 - 580	60- 200	130 - 700	6 - 90	80 - 700	20 - 40	5 - 35	8 - 30
LoD	30		30		3		3	

	Ship		Tower		Ship		Tower	
Fe_E / g s^{-1}	$ClNO_2$ / ppt	Dist.	$ClNO_2$ / ppt	Dist.	$\Delta CO:C_2H_6$	Dist.	$\Delta CO:C_2H_6$	Dist.
Bkgd	<1		<1		NA		NA	
0	<1		<1		4		0	
0.021	0.5 - 2.5	6 - 12	<1	5 - 14	0 - 9	100	5 - 9	>100
0.21	5 - 25	6 - 12	<1	5 - 14	0 - 60	100	10 - 50	100
2.1	30 - 230	6 - 12	<1	5 - 14	30 - 500	>20	100 - 500	>20
LoD	10		10		20		20	

	Ship		Tower		Ship		Tower	
Fe_E / g s^{-1}	$\delta^{13}C(CO)$ / ‰	Dist.	$\delta^{13}C(CO)$ / ‰	Dist.	CH_2O / ppt	Dist.	CH_2O / ppt	Dist.
Bkgd	0		0		NA		NA	
0	<0.1		<0.5		660	70		20
0.021	<0.1		<0.1		660	70	10	20
0.21	0.1 - 0.3	100 - 400	0.2 - 0.4	90 - 370	800	60	190	20
2.1	0.6 - 3	100 - 400	0.6 - 3	100 - 400	1360	10 - 30	960	20
LoD	0.2		0.2		100		100	

Appendix C Model Setup

For the photolysis rates from the MCM subset, the solar zenith angle was set to 1.05 radians, corresponding to the first of June 2023 at 12:00 noon on Barbados. For all other photolysis rates the NCAR TUV calculator (Madronich et al., 2002) has been used to determine the rates for the 12th of November 1996, at 10°N 25°W. In the model, these photolysis rates were multiplied with a number between 0 and 1 that represents a diurnal profile. These input conditions were used to be comparable with van Herpen et al. (2023).

The model was run at 298 K with 70% RH and concentrations of: H_2O = 5.39 $\times 10^{17}$ cm^{-3}, O_2 = 3.94 $\times 10^{18}$ cm^{-3}, H_2 = 1.23 $\times 10^{10}$ cm^{-3}, HCl = 2.55 $\times 10^{9}$ cm^{-3}, DMS = 1.40 $\times 10^{9}$ cm^{-3} and CH_4 = 4.43 $\times 10^{13}$ cm^{-3}. All these concentrations were set as constants except for CH_4. NOx was set using a first-order emission of NO_2, and to set different background O_3 concentrations we either added a first-order emission of O(3P), or we added an extra first order loss rate (by increasing O_3 deposition rate). For the sensitivity analysis, bromine concentrations were set using a first order emission of 400 $cm^{-}3$ $s^{-}1$ Br_2.

An overview of reactions can be found in the supplementary information: reaction_list.xlsx

Acknowledgments

Spark Climate Solutions

Open Research

The reactions and rate coefficients used in the model were obtained from the following sources (*Master Chemical Mechanism, MCM v3.2*, 2023; Seinfeld & Pandis, 2016; Burkholder et al., 2020; Atkinson et al., 2004; Watson et al., 1976; Atkinson et al., 2001, 1997; Madronich et al., 2002; DeMore et al., 1997; Atkinson et al., 2007; Hossaini et al., 2016; Sander et al., 2006; Demore et al., 1994; Daële, V & Poulet, G, 1996; Saiz-Lopez et al., 2014, 2006; Williams et al., 2014; Crawford et al., 1999). The model was built in the compiler program Kintecus (Ianni, 2017).

Author Contributions

Conceived and designed the analysis: MvH, LP, ASL, MSJ; Collected the data: MvH, LP; Contributed data or analysis tools: MvH, LP; Performed the analysis: MvH, LP, CB, TR, MKM, ASL; Wrote the paper: all authors

Conflict of Interest

The University of Copenhagen is pursuing protection of intellectual property related to aspects of this study.

References

Abernethy, S., & Jackson, R. B. (2024). Atmospheric methane removal may reduce climate risks. *Environmental Research Letters*, *19*(5), 051001. doi: 10.1088/1748-9326/ad3b22

Abernethy, S., O'Connor, F. M., Jones, C. D., & Jackson, R. B. (2021). Methane removal and the proportional reductions in surface temperature and ozone. *Philosophical Transactions of the Royal Society A: Mathematical, Physical and Engineering Sciences*, *379*(2210), 20210104. doi: 10.1098/rsta.2021.0104

Agrawal, H., Welch, W. A., Miller, J. W., & Cocker, D. R. (2008). Emission measurements from a crude oil tanker at sea. *Environmental Science & Technology*, *42*(19), 7098-7103. doi: 10.1021/es703102y

Andrés Hernández, M. D., Hilboll, A., Ziereis, H., Förster, E., Krüger, O. O., Kaiser, K., ... Burrows, J. P. (2022). Overview: On the transport and transformation of pollutants in the outflow of major population centres – observational data from the emerge european intensive operational period in summer 2017. *Atmospheric Chemistry and Physics*, *22*(9), 5877–5924. doi: 10.5194/acp-22-5877-2022

Atkinson, R., Baulch, D., Cox, R., Crowley, J., Hampson, R., Hynes, R., ... Troe, J. (2007). Evaluated kinetic and photochemical data for atmospheric chemistry: Volume iii–gas phase reactions of inorganic halogens [Dataset]. *Atmospheric Chemistry and Physics*, *7*(4), 981–1191.

Atkinson, R., Baulch, D., Cox, R., Crowley, J., Hampson Jr, R., Kerr, J., ... Troe, J. (2001). Summary of evaluated kinetic and photochemical data for atmospheric chemistry [Dataset]. *IUPAC Subcommittee on gas kinetic data evaluation for atmospheric chemistry*, *20*.

Atkinson, R., Baulch, D., Cox, R., Hampson Jr, R., Kerr, J., Rossi, M., & Troe, J. (1997). Evaluated kinetic, photochemical and heterogeneous data for atmospheric chemistry: Supplement v. iupac subcommittee on gas kinetic data evaluation for atmospheric chemistry [Dataset]. *Journal of Physical and Chemical Reference Data*, *26*(3), 521–1011.

Atkinson, R., Baulch, D. L., Cox, R. A., Crowley, J. N., Hampson, R. F., Hynes, R. G., ... Troe, J. (2004). Evaluated kinetic and photochemical data for atmospheric chemistry: Volume i - gas phase reactions of o_x, ho_x, no_x and so_x species [Dataset]. *Atmospheric Chemistry and Physics*, *4*(6), 1461–1738. doi: 10.5194/acp-4-1461-2004

Ault, A. P., Gaston, C. J., Wang, Y., Dominguez, G., Thiemens, M. H., & Prather, K. A. (2010). Characterization of the single particle mixing state of individual ship plume events measured at the port of los angeles. *Environmental Science & Technology*, *44*(6), 1954-1961. doi: 10.1021/es902985h

Ausmeel, S., Eriksson, A., Ahlberg, E., Sporre, M. K., Spanne, M., & Kristensson, A. (2020). Ship plumes in the baltic sea sulfur emission control area: chemical characterization and contribution to coastal aerosol concentrations. *Atmospheric Chemistry and Physics*, *20*(15), 9135–9151. doi: 10.5194/acp-20-9135-2020

Baker, A. K., Rauthe-Schöch, A., Schuck, T. J., Brenninkmeijer, C. A. M., van Velthoven, P. F. J., Wisher, A., & Oram, D. E. (2011). Investigation of chlorine radical chemistry in the eyjafjallajökull volcanic plume using observed depletions in non-methane hydrocarbons. *Geophysical Research Letters*, *38*(13). doi: 10.1029/2011GL047571

Baker, A. K., Sauvage, C., Thorenz, U. R., van Velthoven, P., Oram, D. E., Zahn, A., ... Williams, J. (2016, 11). Evidence for strong, widespread chlorine radical chemistry associated with pollution outflow from continental asia. *Scientific Reports*, *6*, 36821. doi: 10.1038/srep36821

Bergamaschi, P., Hein, R., Brenninkmeijer, C. A. M., & Crutzen, P. J. (2000). Inverse modeling of the global co cycle: 2. inversion of 13c/12c and 18o/16o isotope ratios. *Journal of Geophysical Research: Atmospheres*, *105*(D2), 1929-1945. doi: 10.1029/1999JD900819

Burkholder, J., Sander, S., Abbatt, J., Barker, J., Cappa, C., Crounse, J., ... others (2020). *Chemical kinetics and photochemical data for use in atmospheric studies; evaluation number 19* (Tech. Rep.). Jet Propulsion Laboratory, California Institute of Technology, Pasadena CA.

Čampara, L., Hasanspahić, N., & Vujičić, S. (2018). Overview of marpol annex vi regulations for prevention of air pollution from marine diesel engines. In *Shs web of conferences* (Vol. 58, p. 01004).

Chemistry, A. (2024). *Quote for ferrocene price estimate.* Retrieved from `https://www.alfa-chemistry.com` (Accessed: 19-02-2024)

Chen, G., Huey, L. G., Trainer, M., Nicks, D., Corbett, J., Ryerson, T., ... Fehsenfeld, F. (2005). An investigation of the chemistry of ship emission plumes during itct 2002. *Journal of Geophysical Research: Atmospheres*, *110*(D10). doi: 10.1029/2004JD005236

Chen, Y., & Siefert, R. L. (2003). Determination of various types of labile atmospheric iron over remote oceans. *Journal of Geophysical Research: Atmospheres*, *108*(D24). doi: 10.1029/2003JD003515

Cheng, Y., Wang, S., Zhu, J., Guo, Y., Zhang, R., Liu, Y., ... Zhou, B. (2019). Surveillance of so_2 and no_2 from ship emissions by max-doas measurements and the implications regarding fuel sulfur content compliance. *Atmospheric Chemistry and Physics*, *19*(21), 13611–13626. doi: 10.5194/acp-19-13611-2019

Crawford, J., Davis, D., Olson, J., Chen, G., Liu, S., Gregory, G., ... Blake, D. (1999). Assessment of upper tropospheric hox sources over the tropical pacific based on nasa gte/pem data: Net effect on hox and other photochemical parameters [Dataset]. *Journal of Geophysical Research: Atmospheres*, *104*(D13), 16255-16273. doi: 10.1029/1999JD900106

Custard, K. D., Pratt, K. A., Wang, S., & Shepson, P. B. (2016). Constraints on arctic atmospheric chlorine production through measurements and simulations of cl2 and clo. *Environmental Science & Technology*, *50*(22), 12394-12400. doi: 10.1021/acs.est.6b03909

Daële, V, & Poulet, G. (1996). Kinetics and products of the reactions of ch3o2 with cl and clo [Dataset]. *J. Chim. Phys.*, *93*, 1081-1099. doi: 10.1051/jcp/1996931081

DeMore, W., Sander, S., Golden, D., Hampson, R., Kurylo, M., Howard, C., ... Molina, M. (1997). *Chemical kinetics and photochemical data for use in stratospheric modeling. evaluation number 12* (Dataset). Pasadena, CA: Jet Propulsion Laboratory, National Aeronautics and Space ....

Demore, W. B., Sander, S. P., Golden, D. M., Hampson, R. F., Kurylo, M. J., Howard, C. J., ... Molina, M. J. (1994). Chemical kinetics and photochemical data for use in stratospheric modeling: Evaluation number 11 [Dataset]. *Jet Propulsion Laboratory, California Institute of Technology, Pasadena CA*.

De Smedt, I., Theys, N., Yu, H., Danckaert, T., Lerot, C., Compernolle, S., ... Veefkind, P. (2018). Algorithm theoretical baseline for formaldehyde retrievals from s5p tropomi and from the qa4ecv project. *Atmospheric Measurement Techniques*, *11*(4), 2395–2426. doi: 10.5194/amt-11-2395-2018

European Commission, S. . (2023 November 2021, Brussels). *Launch by united states, the european union, and partners of the global methane pledge to keep 1.5c within reach.* Retrieved from `https://ec.europa.eu/commission/presscorner/detail/en/statement_21_5766`

Gorham, K. A., Abernethy, S., Jones, T. R., Hess, P., Mahowald, N. M., Meidan, D., ... Mann, D. (2024). Opinion: A research roadmap for exploring atmospheric methane removal via iron salt aerosol. *Atmospheric Chemistry and Physics*, *24*(9), 5659–5670. doi: 10.5194/acp-24-5659-2024

Hanna, S. R., Briggs, G. A., & Hosker, R. P. (1981). *Handbook on atmospheric diffusion models* (Tech. Rep.). National Oceanic and Atmospheric Administration, Oak Ridge, TN (USA). doi: 10.2172/5591108

Hossaini, R., Chipperfield, M. P., Saiz-Lopez, A., Fernandez, R., Monks, S., Feng, W., ... von Glasow, R. (2016). A global model of tropospheric chlorine chemistry: Organic versus inorganic sources and impact on methane oxidation [Dataset]. *Journal of Geophysical Research: Atmospheres*, *121*(23), 14,271-14,297. doi: 10.1002/2016JD025756

Höglund-Isaksson, L., Gómez-Sanabria, A., Klimont, Z., Rafaj, P., & Schöpp, W. (2020, feb). Technical potentials and costs for reducing global anthropogenic methane emissions in the 2050 timeframe –results from the

gains model. *Environmental Research Communications*, *2*(2), 025004. doi: 10.1088/2515-7620/ab7457

Ianni, J. C. (2017). *Kintecus, windows version 6.01* [Software]. `http://www.kintecus.com`.

Improving performance and emissions characteristics of compression ignition engine: Effect of ferrocene nanoparticles to diesel-biodiesel blend. (2020). *Fuel*, *270*, 117574. doi: 10.1016/j.fuel.2020.117574

IPCC. (2021). Summary for policymakers [Book Section]. In V. Masson-Delmotte et al. (Eds.), *Climate change 2021: The physical science basis. contribution of working group i to the sixth assessment report of the intergovernmental panel on climate change* (pp. 3–32). Cambridge, United Kingdom and New York, NY, USA: Cambridge University Press. doi: 10.1017/9781009157896.001

Ito, A. (2013). Global modeling study of potentially bioavailable iron input from shipboard aerosol sources to the ocean. *Global Biogeochemical Cycles*, *27*(1), 1-10. doi: 10.1029/2012GB004378

Kercher, J. P., Riedel, T. P., & Thornton, J. A. (2009). Chlorine activation by n_2o_5: simultaneous, in situ detection of $clno_2$ and n_2o_5 by chemical ionization mass spectrometry. *Atmospheric Measurement Techniques*, *2*(1), 193–204. doi: 10.5194/amt-2-193-2009

Kim, H. S., Kim, Y. H., & Song, C. H. (2013). Ship-plume sulfur chemistry: Itct 2k2 case study. *Science of The Total Environment*, *450-451*, 178-187. doi: 10.1016/j.scitotenv.2013.01.099

Kivekäs, N., Massling, A., Grythe, H., Lange, R., Rusnak, V., Carreno, S., ... Kristensson, A. (2014). Contribution of ship traffic to aerosol particle concentrations downwind of a major shipping lane. *Atmospheric Chemistry and Physics*, *14*(16), 8255–8267. doi: 10.5194/acp-14-8255-2014

Kleinen, T., Gromov, S., Steil, B., & Brovkin, V. (2021). Atmospheric methane underestimated in future climate projections. *Environmental Research Letters*, *16*(9), 094006. doi: 10.1088/1748-9326/ac1814

Lack, D. A., Corbett, J. J., Onasch, T., Lerner, B., Massoli, P., Quinn, P. K., ... Williams, E. (2009). Particulate emissions from commercial shipping: Chemical, physical, and optical properties. *Journal of Geophysical Research: Atmospheres*, *114*(D7). doi: 10.1029/2008JD011300

Lan, X., Thoning, K., & Dlugokencky, E. (2024). *Trends in globally-averaged ch4, n2o, and sf6 determined from noaa global monitoring laboratory measurements. version 2024-02.* Retrieved 2024-02-11, from `https://doi.org/10.15138/P8XG-AA10`

Lawler, M. J., Sander, R., Carpenter, L. J., Lee, J. D., von Glasow, R., Sommariva, R., & Saltzman, E. S. (2011). Hocl and cl_2 observations in marine air. *Atmospheric Chemistry and Physics*, *11*(15), 7617–7628. doi: 10.5194/acp-11-7617-2011

Le Breton, M., McGillen, M. R., Muller, J. B. A., Bacak, A., Shallcross, D. E., Xiao, P., ... Percival, C. J. (2012). Airborne observations of formic acid using a chemical ionization mass spectrometer. *Atmospheric Measurement Techniques*, *5*(12), 3029–3039. doi: 10.5194/amt-5-3029-2012

Li, Q., Meidan, D., Hess, P., Añel, J. A., Cuevas, C. A., Doney, S., ... others (2023). Global environmental implications of atmospheric methane removal through chlorine-mediated chemistry-climate interactions. *Nature Communications*, *14*(1), 4045. doi: 10.1038/s41467-023-39794-7

Madronich, S., Flocke, S., Zeng, J., Petropavlovskikh, I., & Lee-Taylor, J. (2002). *Tropospheric ultraviolet and visible (tuv) radiation model* [Dataset]. (National Center for Atmospheric Research (NCAR), Boulder, CO)

Marbach, T., Beirle, S., Platt, U., Hoor, P., Wittrock, F., Richter, A., ... Wagner, T. (2009). Satellite measurements of formaldehyde linked to shipping emissions. *Atmospheric Chemistry and Physics*, *9*(21), 8223–8234. doi:

10.5194/acp-9-8223-2009

Marcy, T., Gao, R., Northway, M., Popp, P., Stark, H., & Fahey, D. (2005). Using chemical ionization mass spectrometry for detection of hno3, hcl, and clono2 in the atmosphere. *International Journal of Mass Spectrometry*, *243*(1), 63-70. doi: 10.1016/j.ijms.2004.11.012

Master chemical mechanism, mcm v3.2 [Dataset]. (2023). `http://mcm.leeds.ac.uk/MCM`.

Meidan, D., Li, Q., Cuevas, C. A., Doney, S. C., Fernandez, R. P., van Herpen, M. M. J. W., ... Mahowald, N. M. (2024, apr). Evaluating the potential of iron-based interventions in methane reduction and climate mitigation. *Environmental Research Letters*, *19*(5), 054023. doi: 10.1088/1748-9326/ad3d72

Meyer-Oeste, F. D. (2014). *Troposphere cooling procedure* (No. ES2474420T3).

Mikkelsen, M. K., Liisberg, J. B., van Herpen, M. M. J. W., Mikkelsen, K. V., & Johnson, M. S. (2024). Photocatalytic chloride-to-chlorine conversion by ionic iron in aqueous aerosols: a combined experimental, quantum chemical, and chemical equilibrium model study. *Aerosol Research*, *2*(1), 31–47. doi: 10.5194/ar-2-31-2024

Ming, T., de Richter, R., Dietrich Oeste, F., Tulip, R., & Caillol, S. (2021). A nature-based negative emissions technology able to remove atmospheric methane and other greenhouse gases. *Atmospheric Pollution Research*, *12*(5), 101035. doi: 10.1016/j.apr.2021.02.017

Nisbet, E. G., Manning, M. R., Dlugokencky, E. J., Michel, S. E., Lan, X., Röckmann, T., ... Bromley, T. (2023). Atmospheric methane: Comparison between methane's record in 2006–2022 and during glacial terminations. *Global Biogeochemical Cycles*, *37*(8), e2023GB007875. doi: 10.1029/2023GB007875

Oeste, F. D., de Richter, R., Ming, T., & Caillol, S. (2017). Climate engineering by mimicking natural dust climate control: the iron salt aerosol method. *Earth System Dynamics*, *8*(1), 1–54. doi: 10.5194/esd-8-1-2017

Pathirana, S. L., van der Veen, C., Popa, M. E., & Röckmann, T. (2015). An analytical system for stable isotope analysis on carbon monoxide using continuous-flow isotope-ratio mass spectrometry. *Atmospheric Measurement Techniques*, *8*(12), 5315–5324. doi: 10.5194/amt-8-5315-2015

Pennacchio, L., Mikkelsen, M. K., Krogsbøll, M., van Herpen, M., & Johnson, M. S. (2024, sep). Physical and practical constraints on atmospheric methane removal technologies. *Environmental Research Letters*, *19*(10), 104058. doi: 10.1088/1748-9326/ad7041

Pennacchio, L., van Herpen, M., Meidan, D., Saiz-Lopez, A., & Johnson, M. S. (2024). Catalytic efficiencies for methane removal: Impact of hox, nox and chemistry in the high-chlorine regime. *ACS Earth and Space Chemistry, in peer review*. doi: 10.26434/chemrxiv-2023-3r8sf

Plane, J. M., & Saiz-Lopez, A. (2006). Uv-visible differential optical absorption spectroscopy (doas). In *Analytical techniques for atmospheric measurement* (p. 147-188). John Wiley & Sons, Ltd. doi: 10.1002/9780470988510.ch3

Prados-Roman, C., Fernández, M., Gómez-Martín, L., Cuevas, E., Gil-Ojeda, M., Marusczak, N., ... Saiz-Lopez, A. (2020). Atmospheric formaldehyde at el teide and pic du midi remote high-altitude sites. *Atmospheric Environment*, *234*, 117618. doi: 10.1016/j.atmosenv.2020.117618

Read, K. A., Lee, J. D., Lewis, A. C., Moller, S. J., Mendes, L., & Carpenter, L. J. (2009). Intra-annual cycles of nmvoc in the tropical marine boundary layer and their use for interpreting seasonal variability in co. *Journal of Geophysical Research: Atmospheres*, *114*(D21). doi: 10.1029/2009JD011879

Rogelj, J., & Lamboll, R. D. (2024). Substantial reductions in non-co2 greenhouse gas emissions reductions implied by ipcc estimates of the remaining carbon budget. *Communications Earth & Environment*, *5*. doi: 10.1038/s43247-023-01168-8

Rolph, G., Stein, A., & Stunder, B. (2017). Real-time environmental applications and display system: Ready. *Environmental Modelling & Software*, *95*, 210-228. doi: 10.1016/j.envsoft.2017.06.025

Röckmann, T., van Herpen, M., Brashear, C., van der Veen, C., Gromov, S., Li, Q., ... Johnson, M. S. (2024, jun). The use of δ^{13}c in co to determine removal of ch4 by cl radicals in the atmosphere. *Environmental Research Letters*, *19*(6), 064054. doi: 10.1088/1748-9326/ad4375

Saiz-Lopez, A., Fernandez, R. P., Ordóñez, C., Kinnison, D. E., Gómez Martín, J. C., Lamarque, J.-F., & Tilmes, S. (2014). Iodine chemistry in the troposphere and its effect on ozone [Dataset]. *Atmospheric Chemistry and Physics*, *14*(23), 13119–13143. doi: 10.5194/acp-14-13119-2014

Saiz-Lopez, A., Shillito, J. A., Coe, H., & Plane, J. M. C. (2006). Measurements and modelling of i_2, io, oio, bro and no_3 in the mid-latitude marine boundary layer [Dataset]. *Atmospheric Chemistry and Physics*, *6*(6), 1513–1528. doi: 10.5194/acp-6-1513-2006

Saiz-Lopez, A., & von Glasow, R. (2012). Reactive halogen chemistry in the troposphere. *Chem. Soc. Rev.*, *41*, 6448-6472. doi: 10.1039/C2CS35208G

Sander, S., Friedl, R., Golden, D., Kurylo, M., Moortgat, G., Wine, P., ... others (2006). *Chemical kinetics and photochemical data for use in atmospheric studies evaluation number 15* (Tech. Rep.). Jet Propulsion Laboratory, Pasadena, 2015.

Saueressig, G., Bergamaschi, P., Crowley, J. N., Fischer, H., & Harris, G. W. (1995). Carbon kinetic isotope effect in the reaction of ch4 with cl atoms. *Geophysical Research Letters*, *22*(10), 1225-1228. doi: 10.1029/95GL00881

Seinfeld, J. H., & Pandis, S. N. (2016). *Atmospheric chemistry and physics: from air pollution to climate change* [Dataset]. John Wiley & Sons.

Smith, C., & Mathison, C. (2024, jun). How much methane removal is required to avoid overshooting 1.5°c? *Environmental Research Letters*, *19*(7), 074044. doi: 10.1088/1748-9326/ad5853

Song, C. H., Chen, G., Hanna, S. R., Crawford, J., & Davis, D. D. (2003). Dispersion and chemical evolution of ship plumes in the marine boundary layer: Investigation of o3/noy/hox chemistry. *Journal of Geophysical Research: Atmospheres*, *108*(D4). doi: 10.1029/2002JD002216

Song, C. H., Kim, H. S., von Glasow, R., Brimblecombe, P., Kim, J., Park, R. J., ... Kim, Y. H. (2010). Source identification and budget analysis on elevated levels of formaldehyde within the ship plumes: a ship-plume photochemical/dynamic model analysis. *Atmospheric Chemistry and Physics*, *10*(23), 11969–11985. doi: 10.5194/acp-10-11969-2010

Staniaszek, Z., Griffiths, P. T., Folberth, G. A., O'Connor, F. M., & Archibald, A. T. (2021). Climate and composition impacts of a net-zero anthropogenic methane future using an emissions-driven chemistry-climate model. In *Egu general assembly conference abstracts* (pp. EGU21–5740).

Sturtz, T. M., Jenkins, P. T., & de Richter, R. (2022). Environmental impact modeling for a small-scale field test of methane removal by iron salt aerosols. *Sustainability*, *14*(21). doi: 10.3390/su142114060

Stutz, J., Ackermann, R., Fast, J. D., & Barrie, L. (2002). Atmospheric reactive chlorine and bromine at the great salt lake, utah. *Geophysical Research Letters*, *29*(10), 18-1-18-4. doi: 10.1029/2002GL014812

Tomos, B. A. D., Stamford, L., Welfle, A., & Larkin, A. (2024). Decarbonising international shipping – a life cycle perspective on alternative fuel options. *Energy Conversion and Management*, *299*, 117848. doi: 10.1016/j.enconman.2023.117848

van Herpen, M. M. J. W., Li, Q., Saiz-Lopez, A., Liisberg, J. B., Röckmann, T., Cuevas, C. A., ... Johnson, M. S. (2023). Photocatalytic chlorine atom production on mineral dust–sea spray aerosols over the north atlantic. *Pro-*

ceedings of the National Academy of Sciences, *120*(31), e2303974120. doi: 10.1073/pnas.2303974120

van Herpen, M. M. J. W., Li, S., Bisson, S. E., & Harren, F. J. M. (2002, 08). Photoacoustic trace gas detection of ethane using a continuously tunable, continuous-wave optical parametric oscillator based on periodically poled lithium niobate. *Applied Physics Letters*, *81*(7), 1157-1159. doi: 10.1063/1.1500410

Viollier, E., Inglett, P., Hunter, K., Roychoudhury, A., & Van Cappellen, P. (2000). The ferrozine method revisited: Fe(ii)/fe(iii) determination in natural waters. *Applied Geochemistry*, *15*(6), 785-790. doi: 10.1016/S0883-2927(99)00097-9

von Clarmann, T., & Johansson, S. (2018). Chlorine nitrate in the atmosphere. *Atmospheric Chemistry and Physics*, *18*(20), 15363–15386. doi: 10.5194/acp-18-15363-2018

Wang, X., Jacob, D. J., Eastham, S. D., Sulprizio, M. P., Zhu, L., Chen, Q., ... Liao, H. (2019). The role of chlorine in global tropospheric chemistry. *Atmospheric Chemistry and Physics*, *19*(6), 3981–4003. doi: 10.5194/acp-19-3981-2019

Watson, R., Machado, G., Fischer, S., & Davis, D. D. (1976, 09). A temperature dependence kinetics study of the reactions of Cl (2P3/2) with O3, CH4, and H2O2 [Dataset]. *The Journal of Chemical Physics*, *65*(6), 2126-2138. doi: 10.1063/1.433369

Williams, J. E., Le Bras, G., Kukui, A., Ziereis, H., & Brenninkmeijer, C. A. M. (2014). The impact of the chemical production of methyl nitrate from the no + ch_3o_2 reaction on the global distributions of alkyl nitrates, nitrogen oxides and tropospheric ozone: a global modelling study [Dataset]. *Atmospheric Chemistry and Physics*, *14*(5), 2363–2382. doi: 10.5194/acp-14-2363-2014

Winnes, H., & Fridell, E. (2009). Particle emissions from ships: Dependence on fuel type. *Journal of the Air & Waste Management Association*, *59*(12), 1391-1398. doi: 10.3155/1047-3289.59.12.1391

Wittmer, J., Bleicher, S., Ofner, J., & Zetzsch, C. (2015). Iron (iii)-induced activation of chloride from artificial sea-salt aerosol. *Environmental Chemistry*, *12*(4), 461–475. doi: 10.1071/EN14279

Wittmer, J., Bleicher, S., & Zetzsch, C. (2015). Iron(iii)-induced activation of chloride and bromide from modeled salt pans. *The Journal of Physical Chemistry A*, *119*(19), 4373-4385. doi: 10.1021/jp508006s

Wittmer, J., & Zetzsch, C. (2017). Photochemical activation of chlorine by iron-oxide aerosol. *Journal of Atmospheric Chemistry*, *74*, 187–204. doi: 10.1007/s10874-016-9336-6

Wu, Y., Huo, J., Yang, G., Wang, Y., Wang, L., Wu, S., ... Wang, L. (2023). Measurement report: Production and loss of atmospheric formaldehyde at a suburban site of shanghai in summertime. *Atmospheric Chemistry and Physics*, *23*(5), 2997–3014. doi: 10.5194/acp-23-2997-2023

Yuan, B., Koss, A., Warneke, C., Gilman, J. B., Lerner, B. M., Stark, H., & de Gouw, J. A. (2016). A high-resolution time-of-flight chemical ionization mass spectrometer utilizing hydronium ions (h_3o^+ tof-cims) for measurements of volatile organic compounds in the atmosphere. *Atmospheric Measurement Techniques*, *9*(6), 2735–2752. doi: 10.5194/amt-9-2735-2016

Zhou, F., Zhu, L., Zou, J., & Bai, X. (2023). Tracking and measuring plumes from sailing ships using an unmanned aerial vehicle. *IET Intelligent Transport Systems*, *17*(2), 285-294. doi: 10.1049/itr2.12256

Zhu, X., Prospero, J. M., Savoie, D. L., Millero, F. J., Zika, R. G., & Saltzman, E. S. (1993). Photoreduction of iron(iii) in marine mineral aerosol solutions. *Journal of Geophysical Research: Atmospheres*, *98*(D5), 9039-9046. doi: 10.1029/93JD00202

1135 Zhu, X. R., Prospero, J. M., & Millero, F. J. (1997). Diel variability of soluble
1136 fe(ii) and soluble total fe in north african dust in the trade winds at barbados.
1137 *Journal of Geophysical Research: Atmospheres*, *102*(D17), 21297-21305. doi:
1138 10.1029/97JD01313